The class-IIa HDAC inhibitor TMP269 promotes BMP-Smad signalling and is neuroprotective in *in vitro* and *in vivo* 6-hydroxydopamine models of Parkinson's disease

Adam G. O'Mahony [a], Martina Mazzocchi [a] , Alex Morris [b] , Noelia Morales-Prieto [a] , Caitriona Guinane [b], Sean L. Wyatt [c], Louise M. Collins [a,d], Aideen M. Sullivan [e,f,**] , Gerard W. O'Keeffe [a,f,*]

[a] *Department of Anatomy & Neuroscience, School of Medicine, University College Cork (UCC), Cork, Ireland*
[b] *Department of Biological Sciences, Munster Technological University (MTU), Cork Campus, Cork, Ireland*
[c] *Cardiff School of Biosciences, Cardiff University, Wales, UK*
[d] *Department of Physiology, School of Medicine, UCC, Cork, Ireland*
[e] *Department of Pharmacology and Therapeutics, School of Medicine, UCC, Cork, Ireland*
[f] *APC Microbiome Ireland, UCC, Cork, Ireland*

ARTICLE INFO

ABSTRACT

Degeneration of midbrain nigrostriatal dopaminergic neurons is a pathological hallmark of Parkinson's disease (PD). Peripheral delivery of a compound(s) to arrest or slow this dopaminergic degeneration is a key therapeutic goal. Pan-inhibitors of histone deacetylase (HDAC) enzymes, key epigenetic regulators, have shown therapeutic promise in PD models. However as there are several classes of HDACs (ClassI-IV), class-specific inhibition will be important to ensure target specificity. Here we examine the neuroprotective potential of the Class-IIa HDAC inhibitor, TMP269. We show that TMP269 protected against 6-hydroxydopamine (6-OHDA)-induced neurite injury in SH-SY5Y cells and cultured rat ventral mesencephalic dopaminergic neurons. We find that TMP269 upregulated the neurotrophic factor BMP2 and BMP-Smad dependent transcription signalling in SH-SY5Y cells, which was necessary for its neuroprotective effect against 6-OHDA-induced injury. Furthermore, peripheral continuous infusion of 0.5 mg/kg of TMP269 for 7 days via a mini-osmotic pump, reduced forelimb impairments induced by striatal 6-OHDA administration. TMP269 also protected dopaminergic neurons in the substantia nigra and their striatal terminals from striatal 6-OHDA-induced neurodegeneration and prevented the 6-OHDA-induced increases in the numbers of IBA1-positive microglia in the striatum and substantia nigra *in vivo*. TMP269 also prevented 6-OHDA-induced decreases in BMP2, pSmad1/5 and acetylated histone 3 levels, and it reversed 6-OHDA-induced increase in nuclear HDAC5 in dopaminergic neurons in the substantia nigra. These data add to the growing body of evidence that Class-IIa specific HDAC inhibitors may be pharmacological agents of interest for peripheral delivery with the goal of neuroprotection in PD.

1. Introduction

From a pathophysiological perspective, Parkinson's disease (PD) is characterised by progressive degeneration of midbrain nigrostriatal dopaminergic neurons, and accumulation of aggregates of α-synuclein in the form of Lewy bodies and Lewy neurites, in several affected brain

---

* Corresponding author. Department of Anatomy & Neuroscience, School of Medicine, University College Cork (UCC), Cork, Ireland.
** Corresponding author. Department of Pharmacology and Therapeutics, School of Medicine, UCC, Cork, Ireland.
E-mail addresses: a.sullivan@ucc.ie (A.M. Sullivan), g.okeeffe@ucc.ie (G.W. O'Keeffe).

regions. Loss of midbrain dopaminergic input to the striatum (caudate-putamen) results in the cardinal motor symptoms of PD, and most current therapies are aimed at replacing the lost nigrostriatal dopaminergic neurotransmission (Bloem et al., 2021; Fahn et al., 2004). There are currently no neuroprotective treatments which can slow the gradual worsening of PD neuropathology; therefore, a major research goal is to identify therapies which can target the ongoing neurodegenerative pathology. In particular, neuroprotective drugs that can be administered through a peripheral route is a major goal of current research efforts (Bloem et al., 2021; Kalia et al., 2015).

There is substantial evidence to show that there are alterations in histone acetylation in the *post-mortem* PD brain (Park et al., 2016; Harrison et al., 2019). Because of this, histone deacetylases (HDACs), enzymes that regulate histone acetylation, have been proposed as potential therapies for targeting neurodegeneration in PD (Gupta et al., 2020; Mazzocchi et al., 2020; Sharma et al., 2019). There are four classes of HDACs: Class I (HDAC1, HDAC2, HDAC3 and HDAC8), Class IIa (HDAC4, HDAC5, HDAC7, HDAC9), Class IIb (HDAC6 and HDAC10), Class III (SIRT1-7) and Class IV (HDAC11) (Mazzocchi et al., 2020). Ideal candidates for therapeutic application would be molecules that could be delivered peripherally and cross the blood-brain barrier to reach the degenerating nigrostriatal system. There is some evidence for potential neuroprotective effects of small-molecule HDAC inhibitors (HDIs) in laboratory models of PD. Some studies have shown beneficial effects of pan-HDIs, such as sodium butyrate (NaB) (Rane et al., 2012) and valproic acid (VPA) (Ximenes et al., 2015), in PD models while others have employed class-selective inhibitors, particularly inhibitors of Class I (Choong et al., 2016; Johnston et al., 2013) and Class IIb (Francelle et al., 2020; Dai et al. ; Grozinger et al., 1999; Jian et al., 2017; Li et al., 2021; Pinho et al., 2016) HDACs.

However, there have also been reports of negative effects of HDIs in PD models. For example, it has been reported that the Class III HDI nicotinamide exacerbates neurodegeneration in the lactacystin *in vivo* rat model of PD (Harrison et al., 2015), and some HDAC1/II inhibitors have been shown to exacerbate 1-methyl-4-phenylpyridinium (MPP$^+$)-induced death of cultured dopaminergic neurons (Park et al., 2016). Therefore, there is uncertainty about which of the HDAC classes is the most relevant as a PD target and so it is important to investigate the therapeutic potential of inhibitors of distinct HDAC classes, to ascertain which has most potential in PD therapy.

There is an increasing body of evidence for Class-IIa HDACs being of interest in this regard. In terms of their expression and neuroprotective efficacy, Class IIa HDACs, including HDAC5, are expressed in DA neurons in mouse SN (Mazzocchi et al., 2019; Wu et al., 2017), and gene co-expression studies have shown that HDAC5 and HDAC9, but not HDAC4 and HDAC7, are co-expressed with DA markers in the human SN (Mazzocchi et al., 2019, 2021). Treatment with the Class IIa HDIs, MC1568 and LMK235, have been shown to protect against MPP$^+$- and α-synuclein-induced degeneration of DA neurons *in vitro* (Collins et al., 2015; Mazzocchi et al., 2021), and knockdown of HDAC5, but not HDAC4 and HDAC7, protected against α-synuclein-induced neurite degeneration in SH-SY5Y cells (Mazzocchi et al., 2019).

While these data show the neuroprotective potential of these agents, a key consideration in a PD context is whether peripheral administration of Class-IIa HDIs can exert neuroprotective effects on nigrostriatal neurons *in vivo*. Evidence supporting this possibility comes from studies showing that intraperitoneal (i.p.) administration of the Class IIa-specific HDI, MC1568 (Mai et al., 2005) could reduce HDAC5 levels in the rat nucleus accumbens (Taniguchi et al., 2017), highlighting the feasibility of peripheral administration of HDIs for Class IIa HDAC inhibition in the brain. This is further supported by studies showing that i. p. injection of MC1568 reduced thimerosal-induced apoptosis in rat prefrontal cortex (Guida et al., 2016). Moreover, daily i.p. injection of MC1568 has been shown to reduce forelimb akinesia and partially protect nigral DA neurons and their striatal terminals from 6-OHDA-induced neurodegeneration in adult rats (Mazzocchi et al., 2022).

Although these results are promising, there is a need for further evidence to support the *in vivo* neuroprotective potential of Class-IIa HDIs in *in vivo* models of PD. While the small molecule MC1568 is the most well-characterised Class IIa-specific HDI (Mai et al., 2005), there are other Class-IIa HDIs whose neuroprotective potential in PD models has not been examined. One such compound is TMP269, a novel and selective class IIa HDI with IC50s of 157 nM, 97 nM, 43 nM and 23 nM for HDAC4, HDAC5, HDAC7 and HDAC9, respectively (Lobera et al., 2013). Intraperitoneal administration of TMP269 has been reported to have neuroprotective effects in a rat model of middle cerebral artery occlusion (Su et al., 2020). Moreover, i.p. injection of TMP269 was shown to protect against acute kidney injury in two distinct mouse models (Li et al., 2022).

In order to progress the potential application of Class-IIa HDIs as PD therapeutics, there is a need for information on the molecular mechanisms by which they act on dopaminergic neurons. There is evidence showing that Class-IIa HDIs may upregulate bone morphogenetic protein (BMP) signalling, which is known to be neuroprotective pathway for DA neurons. We have previously shown that MC1568 can upregulate expression of *BMP2* and of its downstream signalling molecule, *SMAD1*, in SH-SY5Y cells (Mazzocchi et al., 2019), and that it can partially protect against 6-hydroxydopamine (6-OHDA)-induced degeneration of SH-SY5Y cells *in vitro* and of adult rat nigrostriatal dopaminergic neurons *in vivo* (Mazzocchi et al., 2022). We have also reported that the HDAC4/5 inhibitor LMK235 promotes BMP-SMAD activation, which is required for the neurite growth-promoting effects of LMK235 on SH-SY5Y cells (Mazzocchi et al., 2021). This is supported by studies showing that HDACs suppress BMP-promoted astrogliogenesis in the developing forebrain (Scholl et al., 2012), and that peripheral administration of TMP269 upregulates BMP7 in acute kidney injury models (Li et al., 2022). Collectively, the available evidence suggests that Class-IIa HDAC inhibition promotes BMP-SMAD signalling, but it is as yet unknown whether BMP-SMAD signalling is required for the neuroprotective effects of Class-IIa HDIs on dopaminergic neurons against 6-OHDA-induced injury.

In the current study, we investigated the potential of TMP269 to protect against the detrimental effects of 6-OHDA in *in vitro* models of PD, and whether any neuroprotective effects of TMP269 required BMP signalling. TMP269 was chosen on the basis that it is a class-IIa HDAC inhibitor (Lobera et al., 2013), and peripheral administration of TMP269 has been shown to be neuroprotective in a rat model of stroke (Su et al., 2020), suggesting that it may exert effects in the brain following peripheral delivery. Given this, in the current study, we also examined the neuroprotective effects of sustained, controlled peripheral infusion of TMP269 via mini-osmotic pump delivery in the intrastriatal 6-OHDA adult rat model of PD.

2. Materials and methods

2.1. Cell culture

SH-SY5Y cells (ATCC; CRL-2266) were cultured in growth media consisting of Dulbecco's Modified Eagle's medium nutrient mixture F-12 (DMEM/F-12) (Sigma), supplemented with 10% heat-inactivated foetal bovine serum (FBS) (Sigma), 100 nM L-Glutamine (Sigma), 100 U/ml Penicillin and 10 μg/ml Streptomycin (Both Sigma), and incubated in a humidified atmosphere at 37 °C and 5% CO_2. Cells were plated at a density of 3×10^4 cells/well in a 24-well tissue culture plate (Sarstedt), or 5×10^4 cells/well in a 24-well plate for transfection. For differentiated SH-SY5Y experiments, cells were cultured in growth media consisting of DMEM-High Glucose (DMEM-HG; Sigma, D5796) supplemented with 10% heat-inactivated foetal bovine serum (FBS), 100 nM L-Glutamine (Sigma), 100U/ml Penicillin and 10 μg/ml Streptomycin (both Sigma). Cells were plated at a density of 1×10^4 cells/well and differentiated as previously described (Taylor-Whiteley et al., 2019). Briefly, cells were treated with 10 μM of retinoic acid (RA)

(Sigma R2625-50 MG) daily for 5 days. Following RA treatment, the media was changed on day 6, replaced with serum-free media, and subsequently cells were treated with 50 ng/ml of brain derived neurotrophic factor (BDNF) (Peprotech 450-02) for the next 7 days before beginning the experiment. For primary cultures, the ventral mesencephalon was dissected from embryonic day (E)14 rat embryos, as previously described (Hegarty et al., 2016), under full ethical approval and licencing. Following dissection, tissue was enzymatically dissociated in a 3:2 solution of HBSS:Trypsin EDTA (both Sigma) and cells were plated at a density of 5×10^4 cells/well in a 24-well tissue culture plate which was pre-coated with 0.1 mg/ml poly-D-lysine (Sigma). Culture media consisted of DMEM/F-12 media, supplemented with D-glucose, 100 nM L-Glutamine (Sigma), 100U/ml Penicillin and 10 μg/ml Streptomycin (Both Sigma), 2% B27 (Gibco), and 1% FBS. Cells were treated with 6-OHDA or TMP269 for up to 72 h at concentrations and treatment regimens as indicated in the Figures and Figure legends.

2.2. Smad signalling activity

To assess BMP Smad signalling pathway activity in response to TMP269 treatment, a Smad GFP reporter assay was used. Briefly, SH-SY5Y cells were transfected using TransIT-X2® reagent (Mirus) with 250 ng of the Cignal GFP Smad reporter plasmid DNA (Qiagen, CCS-017G), and then treated with 0.1 μM TMP269. Cells were then imaged at 48h post-transfection and GFP fluorescence intensity was analysed using ImageJ software (NIH).

2.3. Quantitative real-time PCR (RT-qPCR)

SH-SY5Y cells cultured for 12 h with or without 0.1 μM TMP269 and mRNA was extracted using the RNeasy RNA extraction kit (Qiagen) before being reverse-transcribed and the resulting cDNA amplified by qPCR (Hegarty et al., 2017) using primers and dual-labelled probes for *BMP2, SMAD1, SMAD5, BMPR2, ACVR2A or BMPR1B*. Target mRNA levels were expressed relative to the geometric mean of the reference mRNAs, glyceraldehyde phosphate dehydrogenase (*GAPDH*), Tata binding protein (*TBP*) and β2-microglobulin (*B2M*). The primers were: *BMP2* forward: 5′-GGA GAT TCT TCT TTA ATT TAA G-3′ and reverse: 5′-ACT GCT ATT GTT TCC TAA-3′; *SMAD1* forward: 5′-CCA CTA TAA GAG AGT AGA AAG-3′ and reverse: 5′-CTG GAA AGA ATC TGG AAA-3′; *SMAD5* forward: 5′-ATG CCC AGT ATA TCC AGC-3′ and reverse: 5′-GAA GGA TCT GTG AAT CCA TC-3′; *BMPR2* forward: 5′-TGG GAA AGA AAC AAA TCT G-3′ and reverse: 5′-TGA GGA GGA AGA ATA ATC TG-3′; *ACVR2A* forward: 5′-CCA GCA TCC ATC TCT TGA-3′ and reverse: 5′-GTC GTG ATC CCA ACA TTC-3′; *BMPR1B* forward: 5′-CAC AGA AAG GAA CGA ATG-3′ and reverse: 5′-AGA GCA AAC TAC AGA CAG-3′; *GAPDH* forward: 5′-TGG TCT CCT CTG ACT TCA-3′ and reverse: 5′-GCT GTA GCC AAA TTC GTT G-3′; *TBP* forward: 5′-CTC ACA GAC TCT CAC AAC-3′ and reverse: 5′-AGG TCA AGT TTA CAA CCA A-3′; *B2M* forward: 5′-CCT GAA TTG CTA TGT GTC-3′ and reverse: 5′-CAG TGT AGT ACA AGA GAT AGA-3′. Dual labelled probes were: *BMP2* 5′-FAM-CCC ACG GAG GAG TTT ATC ACC-BHQ1-3′; *SMAD1* 5′-FAM-ACT TCC TCC TGT GCT GGT TCC-BHQ1-3′; *SMAD5* 5′-FAM-AGC CTG TTG CCT ATG AAG AGC C-BHQ1-3′; *BMPR2* 5′-FAM-TCA ATC CAA TGT CTA CTG CTA TGC-BHQ1-3′; *ACVR2A* 5′-FAM-ACA GAG CAT TGC CAT TCC AGC-BHQ1-3′; *BMPR1B* 5′-FAM-ACC TAC ACC CTA CAC TGC CTC-BHQ1-3′.

2.3.1. LDH assay

Where indicated, Lactate dehydrogenase (LDH) assay was performed using the CyQUANT LDH cytotoxicity assay (Thermo Fisher) according to the manufacturer's instructions. Briefly, cell culture media was collected at the experimental end-point and the media was centrifuged at 1500 rpm for 5 min to remove any suspended cells or cellular debris. 50 μl of media was then added per well to a clear, flat-bottomed 96-well plate, before adding an additional 50 μl of the assay substrate mix to each well and incubating in the dark at room temperature for 30min. Following the incubation period, 50 μl of the assay stop solution was then added to each well, before the absorbance in each well was measured at 490 nm and 680 nm using a Multiskan FC Microplate Photometer (Thermo Fisher).

2.4. Immunocytochemistry

For SH-SY5Y cells and primary cultures, cells were fixed using 500 μl of 4% paraformaldehyde per well at room temperature for 15 min. Following fixation, cells received 3 × 5 min washes in 10 mM PBS containing 0.02% Triton X-100 (PBS-T). Non-specific binding was blocked by incubating the cells in 500 μl of 5% bovine serum albumin (BSA) (Sigma) in 10 mM PBS for 1 h at room temperature. Following removal of the blocking solution, 200 μl of a solution containing the primary antibody diluted in 1% BSA in 10 mM PBS was added to the relevant wells and the plate was incubated overnight at 4 °C. The primary antibodies were: tyrosine hydroxylase (TH) (Millipore MAB318; 1:200), BMP2 (Abcam; 1:500) acetylated histone H3 (Santa Cruz Biotechnology sc-56616; 1:200) phosphorylated-Smad (pSmad) 1/5/9 (1:500; Cell Signalling #9516S). Following primary antibody incubation, cells received 3 × 5min washes in PBS-T before being incubated in 200 μl of solution containing the appropriate Alexa Flour 594- or 488-conjugated secondary antibody (1:500; Invitrogen) diluted in 1% BSA in 10 mM PBS, and the plate was incubated at room temperature for 2 h. Then the secondary antibody solution was removed and cells received 3 × 5min washes in PBS-T, before being incubated in 200 μl of solution containing 4′-6-Diamidino-2-phenylindole (DAPI) (1:3000; Sigma) in 10 mM PBS at room temperature for 5 min in the dark. Immunostained SH-SY5Y cells and E14 VM cultures neurons were imaged using an Olympus IX71 inverted microscope. Where indicated, the fluorescence intensity of individual cells was measured by densitometry using ImageJ analysis software.

2.5. Neurite growth analysis

For both SH-SY5Y cells and primary VM culture neurite growth analysis, 5 non-overlapping microscopic fields of view were randomly selected per well per experiment and the images were captured using an Olympus IX71 inverted microscope with an Olympus DP 70 digital camera, and CellSens Dimension software (Olympus). Images were taken at 20× magnification. Neuronal complexity analysis was carried out using ImageJ software (NIH), with the scale calibrated to match the magnification at which the image was taken. For SH-SY5Y cells, neurite length was obtained by measuring the length of the primary neurite from the cell soma. For primary cultures, TH-immunostained neurons were selected in each image for measurement and neurite length was obtained by measuring the length of the primary neurite from the cell soma. A total number of 30 cells were analysed per group per experiment and all experiments were repeated at least three times.

2.6. In vivo study design

32 adult (16 Female, 16 Male) Sprague-Dawley rats were purchased from Envigo, UK, and maintained on a 12h:12h light:dark cycle with access to food and water *ad libitum*. Animals were housed in groups of four in housing cages containing environmental enrichment. Animals were randomly assigned to one of four experimental groups with equal numbers of Females and Males in each group. Experimental groups consisted of: Sham/Vehicle (n = 8), Sham/TMP269 (n = 8), 6-OHDA/Vehicle (n = 8) and 6-OHDA/TMP269 (n = 8). Sham/Vehicle group received stereotactic surgery with a sham injection of saline with 0.01% ascorbate, along with subcutaneous implantation of an Alzet model 2001 mini osmotic pump containing PEG300 and 0.1% DMSO as a vehicle. Sham/TMP269 group received stereotactic surgery with a sham injection of saline with 0.01% ascorbate, along with subcutaneous

implantation of a mini osmotic pump containing PEG300 and TMP269 in 0.1% DMSO. The osmotic pump delivered a continuous daily dose of 0.5 mg/kg TMP269 up to 7 days post implantation. 6-OHDA/Vehicle group received stereotactic injection of 2×10 µg of 6-OHDA in saline with 0.01% ascorbate, along with subcutaneous implantation of a mini osmotic pump containing PEG300 and 0.1% DMSO. 6-OHDA/TMP269 group received stereotactic injection of 2×10 µg of 6-OHDA in saline with 0.01% ascorbate, along with subcutaneous implantation of a mini osmotic pump containing PEG300 and 0.1% DMSO with TMP269 to deliver a daily dose of 0.5 mg/kg TMP269 for up to 7 days post-implantation. This dose of TMP269 was determined based on a study which administered TMP269 in doses of up to 16 mg/kg without any reported toxicity, and which also reported significant increases in histone H2A acetylation in the motor cortex of Sprague-Dawley rats after a single i.p. injection of 1 mg/kg TMP269 (Su et al., 2020). Behavioural testing was performed at one week prior to stereotaxic surgery, and at days 4, 8, and 12 post-surgery. All experiments were conducted in accordance with the European Directive 2010/63/EU and under authorisation granted by the Health Products Regulatory Authority Ireland (AE19130/P182).

2.6.1. Stereotaxic surgery

Stereotaxic surgery was performed under general anaesthesia induced by isoflurane inhalation. Each animal was placed into a stereotactic frame (Stoelting), an incision was made on the skull and two small holes were made into the skull. A two-site unilateral intrastriatal lesion was made by infusion of 6-OHDA hydrobromide (10 µg as free base (Sigma) in 3 µL saline with 0.01% ascorbate, into each of the two sites) at a rate of 1 µL/min with 2 min for diffusion, at the following co-ordinates: AP + 0.4, ML ± 3.1 and AP − 0.4, ML ± 4.3 from bregma, and DV − 5.0 below dura, with incision bar at − 2.3 mm (Surgical co-ordinates as described by Kirik et al., 1998). After diffusion, the needle was withdrawn and sutures were performed. Post-surgery care consisted of animals receiving Meloxicam (1 mg/kg s.c.) as analgesic and 5% glucose solution (i.p.), then placed in an individually housed cage on a heated mat, and kept under observation until fully recovered, before being returned to their home cage.

2.7. Behavioural tests

The cylinder test was used to assess the spontaneous forelimb use of SD rats to evaluate the effect of TMP269 treatment on 6-OHDA induced forelimb asymmetry (Schallert et al., 2000). Briefly, animals were placed in a glass cylinder, and recorded for 5 min. Videos were then analysed using Behavioural Observation Research Interactive Software (BORIS) (University of Torino) where the first 20 independent forelimb touches to the cylinder wall upon full rearing were counted, and simultaneous left and right touches were discounted. Results were expressed as impaired forelimb use as a percentage of the total touches. The stepping test was used to assess forelimb akinesia (Olsson et al., 1995). Briefly, animals were restrained to retain one free forelimb, which was placed on the benchtop. The animal was then moved sideways at a steady pace on the benchtop, across 90 cm in approximately 15 s. The numbers of adjusting steps made by the unrestrained forelimb on both the ipsilateral and contralaterally lesioned sides were counted.

2.8. Tissue collection and processing

Animals were sacrificed at 14 days post-surgery under terminal anaesthesia with sodium pentobarbital (50 mg/kg), and transcardially perfused using 4% paraformaldehyde in 10 mM PBS. Once extracted, brains were placed in 4% paraformaldehyde in 10 mM PBS overnight, then placed in 30% sucrose solution for cryoprotection, before being snap-frozen in isopentane using liquid nitrogen. Cryosections were subsequently cut at 30 µm and placed in cryoprotectant (10 mM PBS with 30% ethylene glycol, 25% glycerol, 20% water) and stored at −20 °C until used for immunohistochemistry.

2.9. Immunohistochemistry

Immunohistochemistry was carried out as previously described (Goulding et al., 2021). Sections were washed three times in 1.2% tris-buffered saline (TBS) solution for 5 min. Sections were quenched using 3% hydrogen peroxide/10% methanol in distilled water for 5 min to block endogenous peroxidase activity, before receiving 3×5min washes in TBS solution. Sections were incubated overnight shaking at 4 °C in TH (Merck Millipore; MAB318 1:500) primary antibody diluted in 1% Tx-TBS serum. Following 3×5min washes in TBS, sections were incubated for 2h in secondary antibody for chromogen detection which consisted of biotinylated horse-anti-mouse IgG (1:200, Vector Labs) diluted in Tx-TBS containing 1% serum. Following 3×5min TBS washes, sections were incubated in streptavidin–biotin–horseradish peroxidase solution (Vector Labs) for 2h. Sections received 3×5min washes in TBS before developing with DAB (Vector Labs). Sections were dehydrated in ethanol, cleared in Xylene, cover-slipped using DPX mounting media (BDH Chemicals) and imaged using the Olympus BX53 Upright Microscope.

Fluorescence microscopy was carried out as previously described (Mazzocchi et al., 2022). Sections were washed three times in Tx-TBS solution for 5 min before being incubated for 1 h at room temperature in a 10% goat serum solution to block non-specific binding. Subsequently, sections were incubated overnight shaking at 4 °C with primary antibodies diluted in 1% serum in TBS. The following primary antibodies were used: TH (Merck Millipore; MAB318 1:1000), HDAC5 (Abcam; ab1439 1:500), Acetylated Histone H3K9 (Sigma; SAB5700141 1:500), BMP2 (Antibodies online; ABIN730903 1:100), and Smad1 pSer463 (Antibodies online; ABIN1714962 1:200). Following three washes in Tx-TBS, sections were incubated for 2h in secondary antibody diluted in TBS containing 1% serum. For fluorescence staining, Alexa Fluor 488-, 594-or 633-conjugated secondary antibodies were used (1:500; Invitrogen). Sections were washed three times in Tx-TBS and nuclei were stained by incubation in DAPI (Sigma; 1:3000) solution for 5 min in the dark, followed by three washes in TBS and cover-slipped using a fluorescent mounting media (Merck Millipore; HC08). Images were acquired using an Olympus BX53 Upright Microscope, and Olympus FV1000 Confocal Laser Scanning Microscope.

2.10. Immunohistochemistry image analysis

To quantify TH immunohistochemistry in the striatum, images were converted to 8-bit images using ImageJ, the segmented line tool was used to trace the outline of the striatum, and mean intensity values were measured to quantify TH-immunopositive staining on the ipsilateral and contralateral sides. To evaluate the numbers of TH-positive neurons in the SN, images were converted to 8-bit images and cell counts were carried out on both the ipsilateral and contralateral sides. Finally to analyse the number of IBA1-positive cells in either SN or striatum in both the ipsilateral and contralateral sides, we used an automated machine learning approach as previously described (Anwer et al., 2023). To quantify nuclear HDAC5 levels in TH-positive neurons in the SN, sections were co-stained for TH, HDAC5 and DAPI. The nuclear outline was traced using the DAPI image of TH-positive cells and used to measure the mean intensity value of the HDAC5 image. A similar approach was used to quantify pSmad1 and AcH3K9 in the nuclei of TH-positive neurons. For BMP2 quantification, the TH-positive neuronal cell body was selected and used to quantify BMP2 levels. All data are presented as percentages of the ipsilateral/contralateral side of the brain.

2.11. Statistical analysis

All statistical analysis was carried out using GraphPad Prism software version 8.3 (©2020 GraphPad Software, CA USA). Statistical

differences between groups were analysed using Student's t-test, one-, two-, or three-way ANOVA as appropriate, with *post-hoc* as indicated in the figure legends. All results were expressed as the mean ± standard error of the mean (SEM) and were considered significant at p < 0.05.

3. Results

3.1. TMP269 increases histone acetylation and decreases HDAC5 activity in SH-SY5Y cells

In this study, we evaluated the neurotrophic potential of the Class IIa-specific HDAC inhibitor, TMP269 (Fig. 1A), which inhibits each of Class IIa HDAC subtypes, HDAC 4, 5, 7 and 9, with IC$_{50}$ of 126, 80, 36, and 9 nM, respectively (Lobera et al., 2013). We first evaluated the potential of TMP269 to increase the levels of histone acetylation, using immunocytochemical staining for nuclear histone acetylation, as a readout of successful HDAC inhibition. We found a significant increase in the nuclear levels of acetylated histone 3 (acH3-K9.K14) in SH-SY5Y cells after treatment with 0.1 μM TMP269 for 72h (Fig. 1B and C). We then used a HDAC5-specific enzymatic assay to confirm that TMP269 significantly reduced HDAC5 activity (Fig. 1D). Collectively, these data show that treatment with TMP269 significantly increased histone acetylation and reduced HDAC5 activity in SH-SY5Y cells.

3.2. TMP269 protects against 6-OHDA-induced reductions in neurite growth in SH-SY5Y cells and cultured dopaminergic neurons

We next sought to determine whether treatment with TMP269 could protect against 6-OHDA-induced reductions in neurite growth, as a single-cell readout of cellular injury. We used a concentration of 5 μM 6-OHDA, which induces neurite injury without adversely affecting cell viability, to ensure that differences in the former were not secondary to the latter. The concentration and time of 6-OHDA treatment was chosen based on the results of a previous study showing that 5 μM 6-OHDA treatment for 72h resulted in significant reductions in neurite growth without an adverse effect on cell viability in SH-SY5Y cells (Anantha et al., 2022). Firstly, SH-SY5Y cells were treated concurrently with or without 5 μM 6-OHDA and increasing concentrations (0, 0.01, 0.1, 1 μM) of TMP269 daily for 72h (Fig. 2A). One-way ANOVA revealed a significant effect of treatment (F$_{(4, 25)}$ = 10.92, P < 0.001). *Post-hoc* testing showed that 6-OHDA induced a significant decrease in neurite growth compared to the control group, which was prevented by concurrent TMP269 treatment at concentrations of 0.1 μM and 1 μM (Fig. 2B–G). There was no significant effect of treatment on cell viability (F$_{(4, 10)}$ =

1.042, P = 0.43) as measured using LDH assay (Fig. 2C).

We next employed a delayed treatment paradigm, wherein SH-SY5Y cells were treated with or without 5 μM 6-OHDA for an initial 24h period, before addition of the lowest effective TMP269 dose of 0.1 μM daily for a further 72h (Fig. 2D). One-way ANOVA showed a significant effect of treatment (F$_{(2, 9)}$ = 37.86, P < 0.0001). *Post-hoc* testing showed that 6-OHDA induced a significant decrease in neurite growth compared to the control group, which was prevented by delayed TMP269 treatment (Fig. 2E–G). There was no significant effect of treatment on cell viability (F$_{(2, 9)}$ = 37.86, P < 0.0001) in the LDH assay (Fig. 2F).

We next differentiated SH-SY5Y cells using a 12-day differentiation protocol that has been shown to increase β-III tubulin and TH expression in these cells (Taylor-Whiteley et al., 2019). To do this, SH-SY5Y cells were cultured in the presence of 10 μM RA and 50 ng/ml BDNF for 12 days, which resulted in a high level of TH expression in these cells (Fig. 3A). Cells were then treated concurrently with or without 5 μM 6-OHDA and 0.1 μM TMP269 on days 13, 14 and 15, and neurite length and LDH were assessed on day 16. One-way ANOVA showed a significant effect of treatment on neurite length (F$_{(2, 6)}$ = 23.23, P < 0.01). *Post-hoc* testing showed that 6-OHDA-induced a significant decrease in neurite growth compared to the control group, which was prevented by TMP269 treatment (Fig. 3B). There was no significant effect of treatment on cell viability (F$_{(2, 9)}$ = 37.86, P < 0.0001) in the LDH assay (Fig. 3C).

Although SH-SY5Y cells are a useful tool for drug screening and molecular analyses, they do not recapitulate all features of dopaminergic neurons. Therefore, we repeated the initial 'concurrent TMP269' experiment in primary cultures of dopaminergic neurons. Specifically, primary cultures of E14 rat VM were established and treated concurrently with or without 5 μM 6-OHDA and 0.1 μM TMP269 daily for 72h, then neurite length of tyrosine hydroxylase (TH)-positive dopaminergic neurons in these cultures was analysed. One-way ANOVA showed a significant effect of treatment (F$_{(2, 6)}$ = 23.23, P < 0.01). *Post-hoc* testing showed that 6-OHDA induced a significant decrease in neurite growth compared to the control group, which was prevented by TMP269 treatment (Fig. 3D and E). Collectively, these data show that TMP269 protects against 6-OHDA-induced neurite injury *in vitro*.

3.3. TMP269 increases BMP2 expression and promotes BMP-Smad-dependent transcription in SH-SY5Y cells

Our previous work has implicated Class-IIa HDACs as regulators of the BMP-Smad pathway (Mazzocchi et al., 2019), and the neurotrophic factor BMP2 (Goulding et al., 2019) has been has been identified by Chip-Seq analysis as a HDAC5 target gene (Taniguchi et al., 2017). This
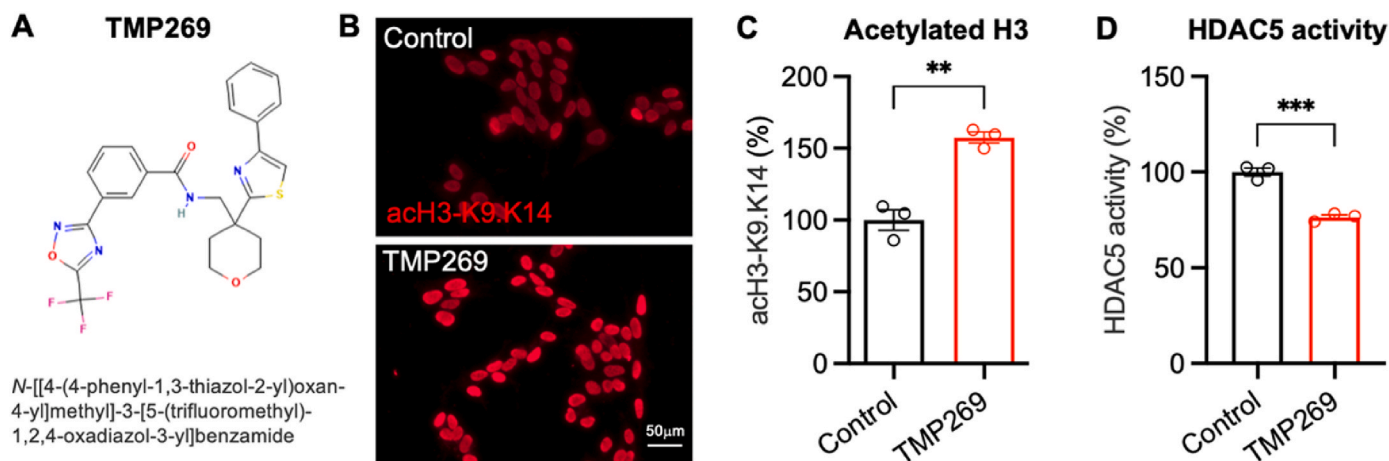
Fig. 1. TMP269 increases histone acetylation and decreases HDAC5 activity in SH-SY5Y cells. **(A)** Structure and IUPAC name of TMP269 (PubChem ID = 53344908; accessed on Jan 13, 2024 https://pubchem.ncbi.nlm.nih.gov/compound/tmp269). **(B)** Representative photomicrographs and **(C)** graph of acetylated histone 3 (acH3-K9.K14) in SH-SY5Y cells cultured with or without 0.1 μM TMP269 for 72h. Scale bar = 50 μm. **(D)** Graph of HDAC5 enzyme activity in SH-SY5Y cells cultured with or without 0.1 μM TMP269. All data are presented as mean ± SEM from *n* = 3 independent experiments. **p < 0.01, ***p < 0.001; Student's t-test.
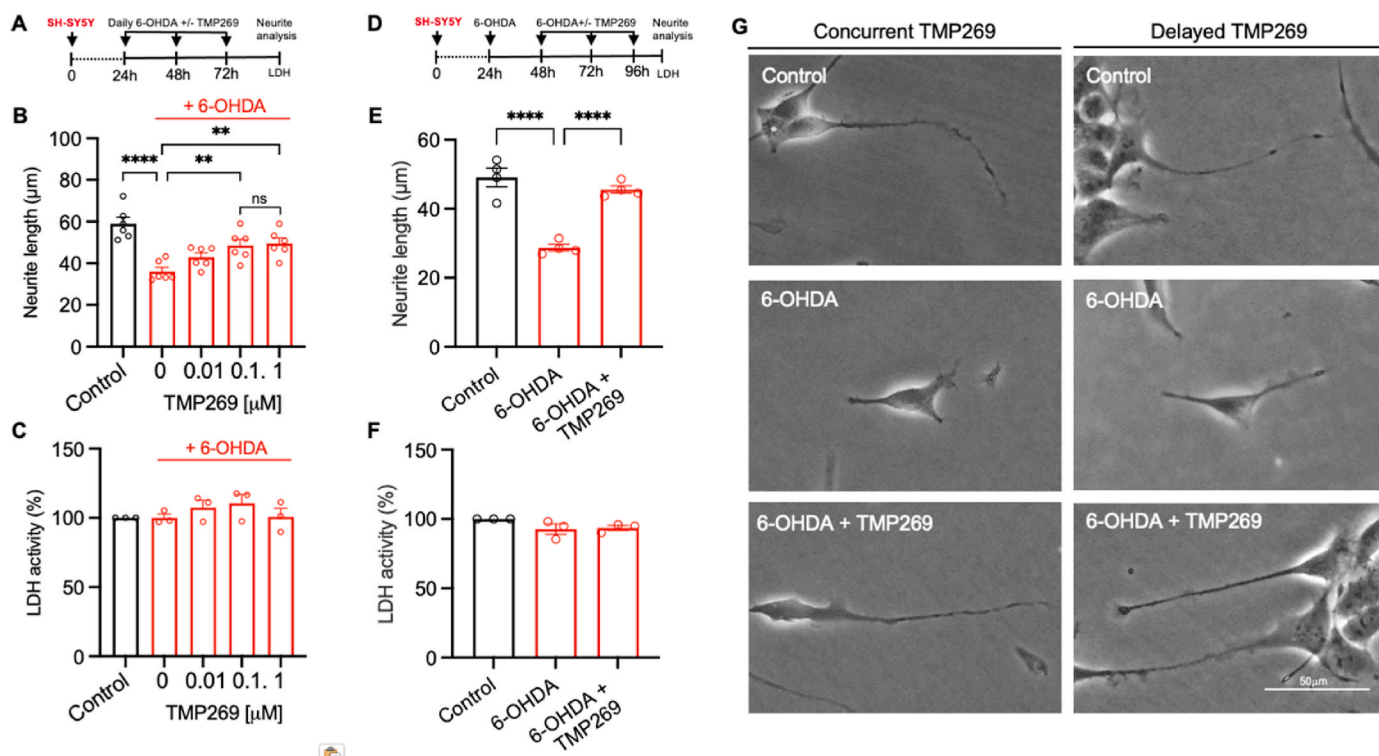
Fig. 2. TMP269 protects against 6-OHDA-induced reductions in neurite growth in SH-SY5Y cells. **(A)** Schema of the treatment regime used in B and C. **(B)** Neurite length and **(C)** LDH activity of SH-SY5Y cells treated concurrently with or without 5 μM 6-OHDA and increasing concentrations of TMP269 (0, 0.01, 0.1 and 1 μM) daily ('concurrent TMP269') for 72h. **(D)** Schema of the treatment regime used in E and F. **(E)** Neurite length and **(F)** LDH activity of SH-SY5Y cells treated with or without 5 μM 6-OHDA for an initial 24h period before addition of 0.1 μM TMP269 daily ('delayed TMP269') for a further 72h. **(G)** Representative photomicrographs of SH-SY5Y cells for the concurrent and delayed TMP269 experiments. Scale bar = 50 μm. All data are presented as the mean ± SEM from $n = 3–6$ independent experiments. *p < 0.05, ****p < 0.0001; One-way ANOVA with *post-hoc* Tukey test.

is of interest given the known neuroprotective effects of BMP ligands on dopaminergic neurons (Goulding et al., 2021; Vitic et al., 2021). These studies, combined with our finding here that TMP269 has an HDAC5 inhibitory effect in SH-SY5Y cells (Fig. 1D), suggested that TMP269 treatment may increase BMP2 expression. To investigate this, SH-SY5Y cells were treated for 24 h with 0.1 μM TMP269, and RT-qPCR was used to examine the expression of *BMP2* and of multiple components of the BMP pathway, including the BMP receptors (*BMPR2* and *BMPR1B*) and R-Smads transcription factors (*SMAD1* and *SMAD5*) (Fig. 4A). TMP269 treatment significantly increased the expression *BMP2* (Fig. 4B), without affecting the expression of other components of the BMP-Smad pathway (Fig. 4C–F).

To determine if TMP269 had an effect on BMP-Smad dependent transcription, SH-SY5Y cells were transfected with a Smad-GFP reporter construct in which GFP expression is under the control of a BMP-responsive element (BRE-GFP) (Fig. 4G), and were cultured with or without 0.1 μM TMP269. Quantification of GFP fluorescence (as a read-out of BMP-Smad dependent transcription) revealed a significant increase in the TMP269-treated group after 24 h, indicating a BMP-Smad-dependent transcriptional response (Fig. 4H). Collectively, these data suggest that the BMP-Smad pathway may be involved in the beneficial effects of TMP269 on 6-OHDA-induced neurite injury.

3.4. TMP269 increases BMP2 and pSmad1/5 expression and protects against 6-OHDA-induced decreases in neurite growth through the BMP-Smad pathway in SH-SY5Y cells

To confirm these findings and to examine their functional relevance, we next examined BMP2 and pSmad1 levels in SH-SY5Y cells treated concurrently with or without 5 μM 6-OHDA and or 0.1 μM TMP269 daily for 72h. We found a significant mains effect of TM269 ($F_{(1, 8)} = 26.65$, P

= 0.0009) but not of 6-OHDA ($F_{(1, 8)} = 0.467$, P = 0.514) on BMP2 expression in SH-SY5Y cells, with no significant 6-OHDA x TMP269 interaction ($F_{(1, 8)} = 0.016$, P = 0.903) (Fig. 5A and B). *Post-hoc* testing revealed a significant increase in BMP2 expression in both TMP269-treated groups relative to the controls (Fig. 5A and B). In terms of cellular localisation, BMP2 immunoreactivity was evident in the nuclei and cytoplasm, as has been previously reported for BMP2 (Cordner et al., 2017) and for other members of the BMP family (Osorio et al., 2013). We also examined phospho(p)Smad1 expression since BMP2 is known to increase nuclear pSmad1/5 levels (Hegarty et al., 2014; Hegarty et al., 2013). We found a significant mains effect of TM269 ($F_{(1, 12)} = 12.79$, P = 0.0038), but not of 6-OHDA ($F_{(1, 8)} = 0.467$, P = 0.514), on pSmad1/5 levels in SH-SY5Y cells, with no significant 6-OHDA x TMP269 interaction ($F_{(1, 8)} = 0.204$, P = 0.659) (Fig. 5C and D). *Post-hoc* testing revealed a significant increase in nuclear pSmad1/5 immuno-reactivity in both TMP269-treated groups relative to the controls (Fig. 5C and D).

To determine if the beneficial effect of TMP269 on 6-OHDA-induced decreases in neurite growth was mediated through the BMP-Smad pathway, we examined neurite growth in SH-SY5Y cells treated daily for 72 h with 0.1 μM TMP269, with or without 5 μM 6-OHDA, and with or without 1 μg/ml of the BMPR1 inhibitor dorsomorphin, which blocks BMP-Smad signalling (Yu et al., 2008). A two-way ANOVA revealed a significant Dorsomorphin × treatment interaction ($F_{(2, 12)} = 31.5$, P < 0.001) (Fig. 5E and F). *Post-hoc* testing revealed that 6-OHDA caused a significant reduction in neurite growth, that was completely prevented by TMP-269 treatment (Fig. 5E and F). This beneficial effect of TMP-269 on 6-OHDA-induced decreases in neurite growth was completely absent when cells were co-treated with dorsomorphin (Fig. 5E and F). Collectively, these data show that TMP269 activates the BMP-Smad pathway, and that this is necessary for TMP269 to prevent the detrimental effects
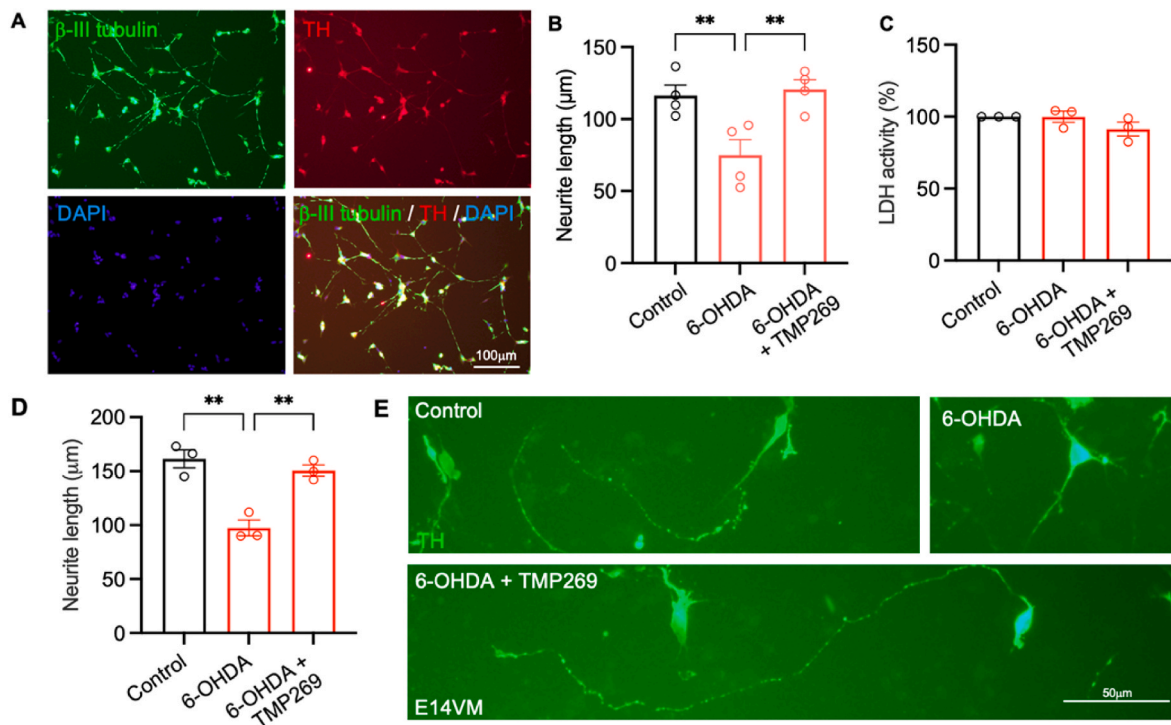
Fig. 3. TMP269 protects against 6-OHDA-induced reductions in neurites of cultured dopaminergic neurons. **(A)** Representative photomicrographs of SH-SY5Y cells after a 12-day dopaminergic differentiation protocol, immunostained for βIII-tubulin (green), tyrosine hydroxylase-positive (TH; red) and counterstained with DAPI (blue). Scale bar = 100 μm. **(B)** Graphs of neurite length of TH-positive cells and **(C)** LDH activity in these differentiated SH-SY5Y cultures. **(D)** Graph and **(E)** representative photomicrographs of neurite length in primary cultures of E14 rat VM treated concurrently with or without 5 μM 6-OHDA and 0.1 μM TMP269 daily for 72h. Scale bar = 50 μm. All data are presented as the mean ± SEM from n = 3 independent experiments. **p < 0.01; One-way ANOVA with *post-hoc* Tukey test. (For interpretation of the references to colour in this figure legend, the reader is referred to the Web version of this article.)

of 6-OHDA on neurite growth.

3.5. Peripheral infusion of TMP269 partially improves 6-OHDA-induced motor dysfunction

We next performed an *in vivo* experiment to determine whether infusion of TMP269 could ameliorate 6-OHDA-induced impairments in motor function and nigrostriatal neurodegeneration. For detailed description of the experimental design see the Methods section. In brief, a mixed cohort of adult male and female rats (n = 8 total per group; 4 male and 4 female) received unilateral intrastriatal stereotactic injection of 6-OHDA or saline, followed by subdermal implantation of a mini-osmotic pump delivering a daily concentration of 0.5 mg/kg TMP269 or vehicle (Fig. 6A). Motor behaviour was assessed using the stepping (Olsson et al., 1995) and cylinder (Schallert et al., 2000) tests of sensorimotor function based on asymmetric forelimb use, at baseline (one day before surgery) and on days on days 4, 8 and 12 post-surgery (Fig. 6A). As expected, there was no significant effect of time ($F_{(3, 84)}$ = 0.527, P = 0.2083), 6-OHDA ($F_{(1, 28)}$ = 3.911, P = 0.057) or TMP269 treatment ($F_{(1, 28)}$ = 3.097, P = 0.0893) on the number of steps taken with the ipsilateral paw in the stepping test (Fig. 6B). However, there was a significant effect 6-OHDA × TMP269 interaction ($F_{(1, 28)}$ = 10.53, P = 0.003), on the number of steps taken with the contralateral paw. *Post-hoc* testing revealed that rats of the 6-OHDA + TMP269 group took significantly more steps than those of the 6-OHDA + vehicle group with the contralateral paw at day 8 and day 12 post-surgery (Fig. 6C).

In the cylinder test, since there was a significant 6-OHDA x time interaction ($F_{(3, 84)}$ = 4.050, P = 0.0097), we performed *post-hoc* testing, and at 12 days post-surgery, there was a significant reduction in contralateral paw use in the 6-OHDA + vehicle group that was not seen in the 6-OHDA + TMP269 group relative to the controls (Fig. 6D). While there was no significant difference between the 6-OHDA + vehicle and

the 6-OHDA + TMP269 groups, the latter had a tendency of more contralateral forelimb use at 12 days post-surgery (8.75 ± 4.88% v 28.75 ± 9.32% respectively). Collectively these data show that peripheral administration of TMP269 partially improves motor function in 6-OHDA-lesioned rats.

3.6. Peripheral infusion of TMP269 prevents 6-OHDA-induced nigrostriatal degeneration

We next sought to examine if the improvements in motor function translated into improvements in nigrostriatal integrity by analysing the numbers of TH-positive neurons in the SN and TH-positive innervation of the striatum. There was a significant 6-OHDA × TMP269 interaction ($F_{(1, 28)}$ = 46.82, P < 0.0001) on the number of TH-positive neurons in the SN. *Post-hoc* testing revealed a significant decrease in the numbers of TH-positive cells in the SN in 6-OHDA + vehicle group which was not see in the 6-OHDA + TMP269 group (Fig. 7A and B). Similarly there was a significant 6-OHDA × TMP269 interaction ($F_{(1, 28)}$ = 46.82, P < 0.0001) on the TH-positive terminals in the striatum. *Post-hoc* testing revealed a significant decrease in TH-positive innervation in the striatum in 6-OHDA + vehicle group which was not see in the 6-OHDA + TMP269 group (Fig. 7C and D). Collectively these data show that peripheral administration of TMP269 protects against 6-OHDA-induced nigrostriatal degeneration.

3.7. Peripheral infusion of TMP269 prevents the 6-OHDA-induced microglial response

We next examined whether TMP269 mitigated the 6-OHDA-induced microglia response by counting the numbers of IBA1+ microglia in the SN and striatum as a proxy measure for neuroinflammation (Thakur et al., 2017). In the SN we found a significant effect of 6-OHDA ($F_{(1, 28)}$
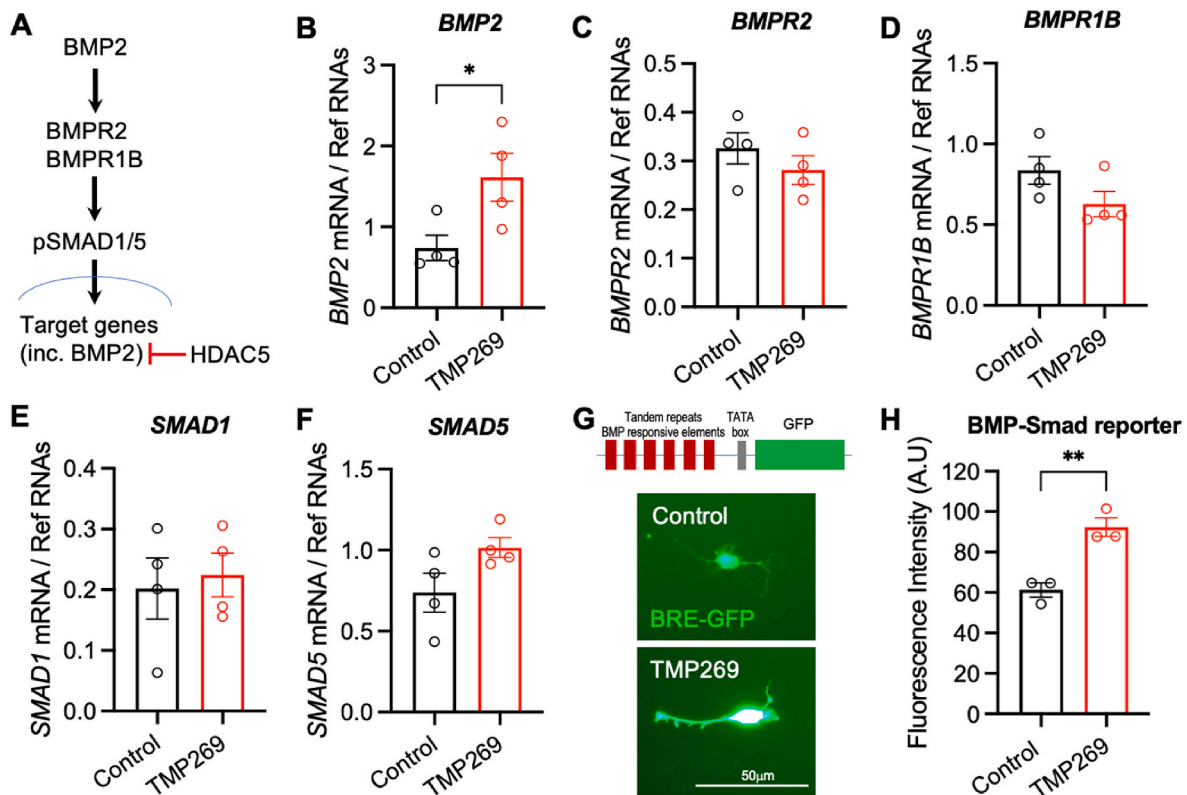
Fig. 4. TMP269 increases *BMP2* expression and promotes BMP-Smad-dependent transcription in SH-SY5Y cells. **(A)** Schema showing the BMP-Smad pathway and illustrating that HDAC5 binds to the BMP2 promoter. **(B–F)** Graphs showing RT-qPCR data for **(B)** *BMP2*, **(C)** *BMPR2*, **(D)** *BMPR1B*, **(E)** *SMAD1* and **(F)** *SMAD5* mRNA levels relative to the levels of the geometric mean of three reference mRNAs, *GAPDH*, *TBP* and *B2M*, in SH-SY5Y cells treated for 24 h with 0.1 μM TMP269. **(G)** Schema showing the BRE-GFP reporter and representative photomicrographs of BRE-GFP-transfected SH-SY5Y cells, with and without TMP269 treatment. Scale bar = 50 μm. **(H)** Graph showing densitometric quantification of GFP fluorescence intensity in SH-SY5Y cells, with and without TMP269 treatment. All data are presented as the mean ± SEM from $n = 3$ or 4 independent experiments. *$p < 0.05$, **$p < 0.01$; Student's t-test.

= 22.03, P < 0.0001) and TMP269 ($F_{(1, 28)}$ = 19.44, P < 0.001) as well as 6-OHDA x TMP269 interaction ($F_{(1, 28)}$ = 14.09, P < 0.001) on the number of IBA1+ cells in the SN. Planned *post-hoc* comparisons revealed a significant increase in the numbers of IBA1+ cells in the SN in the 6-OHDA + vehicle group which was prevented by TMP269 (Fig. 8A and B).

Similarly, in the striatum there was a significant mains effect of 6-OHDA ($F_{(1, 28)}$ = 157.9, P < 0.0001) and TMP269 ($F_{(1, 28)}$ = 144.8, P < 0.001) as well as 6-OHDA x TMP269 interaction ($F_{(1, 28)}$ = 102.3, P < 0.001) on the number of IBA1+ cells in the striatum. Planned *post-hoc* comparisons revealed a significant increase in the numbers of IBA1+ cells in the striatum in the 6-OHDA + vehicle group, which was prevented by TMP269 (Fig. 8C and D). Collectively, these data show that peripheral infusion of TMP269 prevents the 6-OHDA-induced microglial response *in vivo*.

3.8. TMP269 prevents 6-OHDA-induced decreases in BMP2 and pSmad1/5 in the SN in vivo

As we had demonstrated that TMP269 increases BMP2 and pSmad1/5 expression in SH-SY5Y cells, we next examined whether changes in BMP2 and pSmad1/5 expression were observed in the SN *in vivo*. In the SN we found a significant effect of 6-OHDA ($F_{(1, 20)}$ = 15.01, P = 0.0009) and TMP269 ($F_{(1, 20)}$ = 13.16, P = 0.0117) as well as a 6-OHDA x TMP269 interaction ($F_{(1, 20)}$ = 7.41, P = 0.013) on BMP2 expression in TH-positive DA neurons in the SN (Fig. 9A). Planned *post-hoc* comparisons revealed a significant decrease in BMP2 expression in TH-positive DA neurons in the SN of the 6-OHDA + vehicle group, which was prevented by TMP269 (Fig. 9A).

To confirm these findings, we also examined levels of pSmad1/5. We found a significant effect of 6-OHDA ($F_{(1, 20)}$ = 17.09, P = 0.0005) and TMP269 ($F_{(1, 20)}$ = 6.641, P = 0.018) as well as a 6-OHDA x TMP269 interaction ($F_{(1, 20)}$ = 9.59, P = 0.0057) on the levels of pSmad1/5 in TH-positive DA neurons in the SN (Fig. 9B). As was observed with BMP2, planned *post-hoc* comparisons revealed a significant decrease in pSmad1/5 expression in the SN of the 6-OHDA + vehicle group, which was prevented by TMP269 (Fig. 9B). Collectively these data show that 6-OHDA induced decreases in BMP2 and pSmad1/5 levels in TH-positive DA neurons in the SN *in vivo*, and that this was prevented by peripheral delivery of TMP269.

3.9. TMP269 prevents 6-OHDA-induced alterations in nuclear HDAC5 and acetylated histone 3 in the SN in vivo

Finally, we assessed the levels of nuclear HDAC5 and acetylated H3 in TH-positive DA neurons in the SN *in vivo*. We found a significant effect of 6-OHDA ($F_{(1, 20)}$ = 17.09, P = 0.0005) and TMP269 ($F_{(1, 20)}$ = 6.641, P = 0.018) as well as a significant 6-OHDA x TMP269 interaction ($F_{(1, 20)}$ = 14.76, P = 0.001) on nuclear HDAC5 expression in the SN (Fig. 9C). Planned *post-hoc* comparisons revealed a significant increase in nuclear HDAC5 in TH-positive neurons in the SN of the 6-OHDA + vehicle group, which was prevented by TMP269 (Fig. 9C).

There was also a significant 6-OHDA x TMP269 interaction ($F_{(1, 20)}$ = 12.87, P = 0.0018) on acetylated H3 expression (Fig. 9D). Planned *post-hoc* comparisons revealed a significant decrease in acetylated H3 levels in TH-positive neurons in the SN of the 6-OHDA + vehicle group, which was prevented by TMP269 treatment (Fig. 9D).
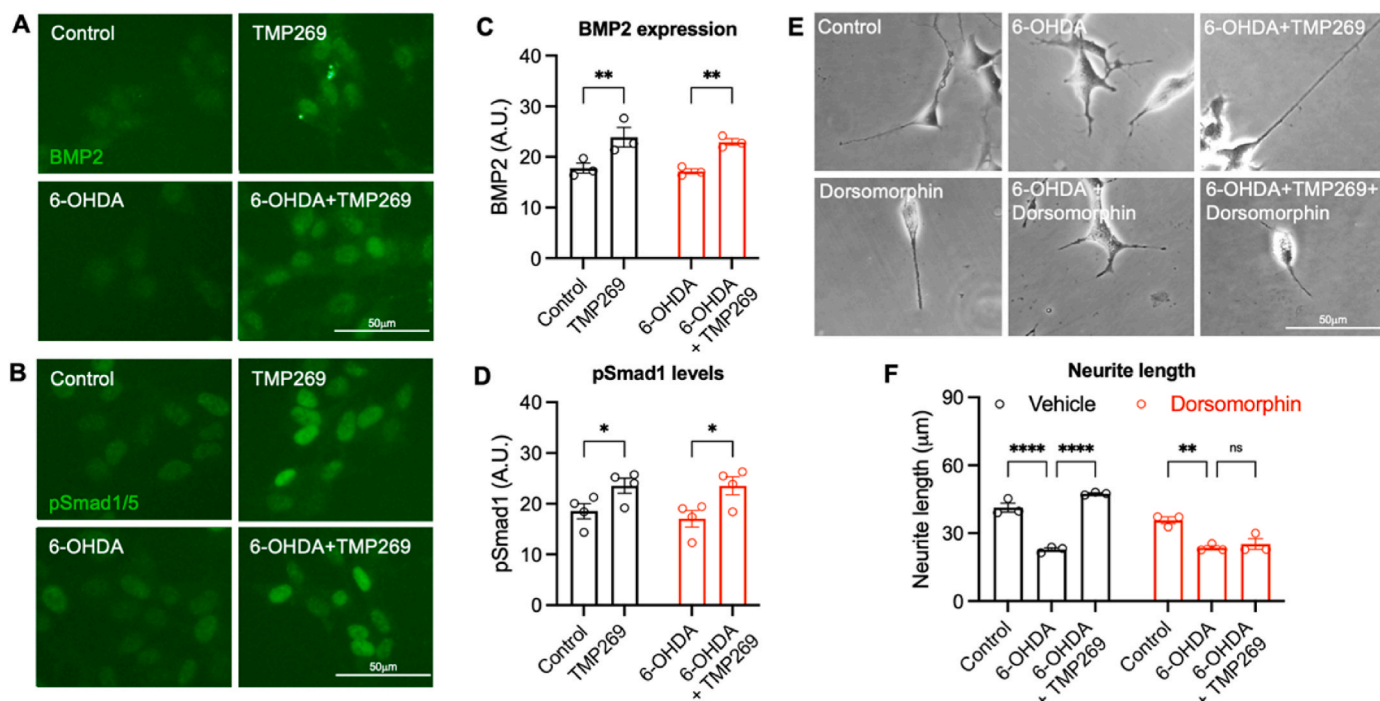
Fig. 5. TMP269 increases BMP2 and pSmad1/5 expression and protects against 6-OHDA-induced decreases in neurite growth through the BMP-Smad pathway in SH-SY5Y cells. Representative photomicrographs of SH-SY5Y cells treated with 5 μM 6-OHDA and cultured with or without 0.1 μM TMP269 for 72h before immuno-staining for (**A**) BMP2 or (**C**) pSmad1/5. Densitometric quantification of (**B**) BMP2 expression and (**D**) pSmad1/5 in SH-SY5Y cells treated with 5 μM 6-OHDA and cultured with or without 0.1 μM TMP269 for 72h. (**E**) Representative photomicrographs and (**F**) neurite length analysis of SH-SY5Y cells treated with 5 μM 6-OHDA and cultured with or without 0.1 μM TMP269 and with or without 1 μg/ml dorsomorphin for 72h. Scale bar = 50 μm. All data are presented as the mean ± SEM from $n = 3$–4 independent experiments. *$p < 0.05$, **$p < 0.01$, ****$p < 0.0001$; Two-way ANOVA with *post-hoc* Tukey's test.
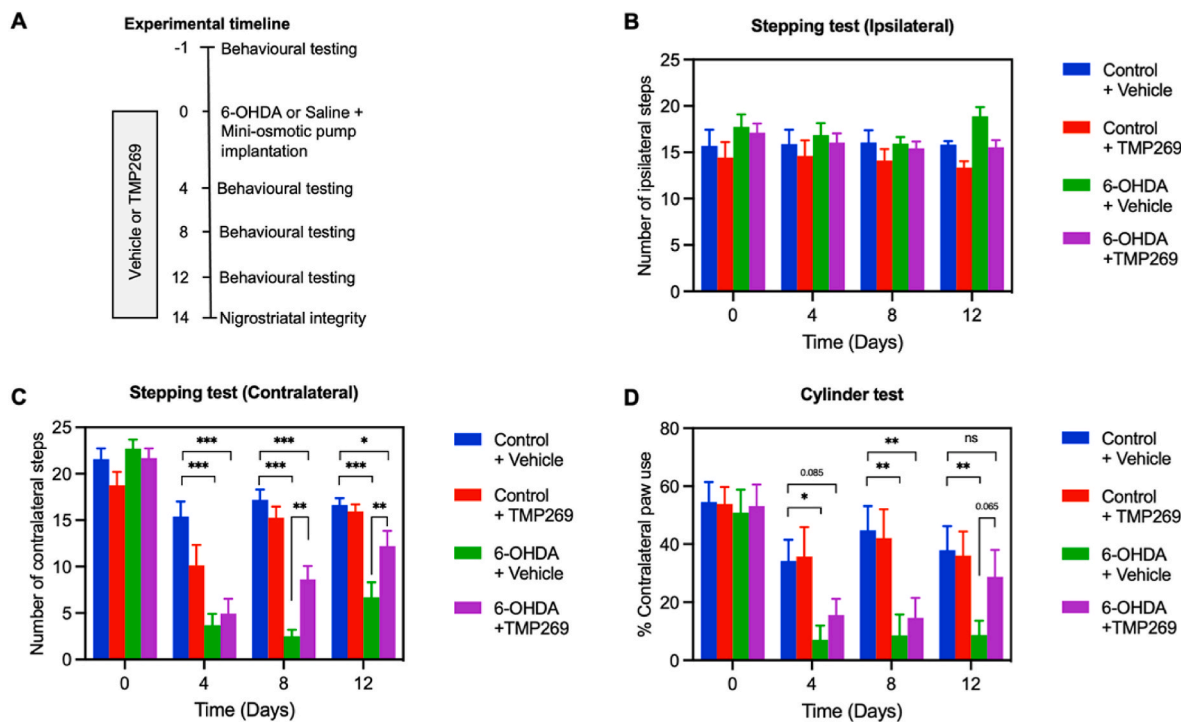
Fig. 6. Peripheral administration of TMP269 partially improves motor function in 6-OHDA-lesioned rats. (**A**) Schema showing the experimental design in which a daily dose of 0.25 mg/kg TMP269 daily was delivered via a mini-osmotic pump starting the same day as intrastriatal 6-OHDA lesion. (**B, C**) Graphs showing the numbers of adjusting steps on the Stepping test made by the (**B**) ipsilateral (unaffected) paw and (**C**) the contralateral (affected) paw. (**D**) Graph showing the percentage of contralateral paw use in the cylinder test. All data are presented as the mean ± SEM of $n = 8$ per group. ***$p < 0.001$, **$p < 0.01$, *$p < 0.05$; Three-way ANOVA with *post-hoc* Fishers LSD test.
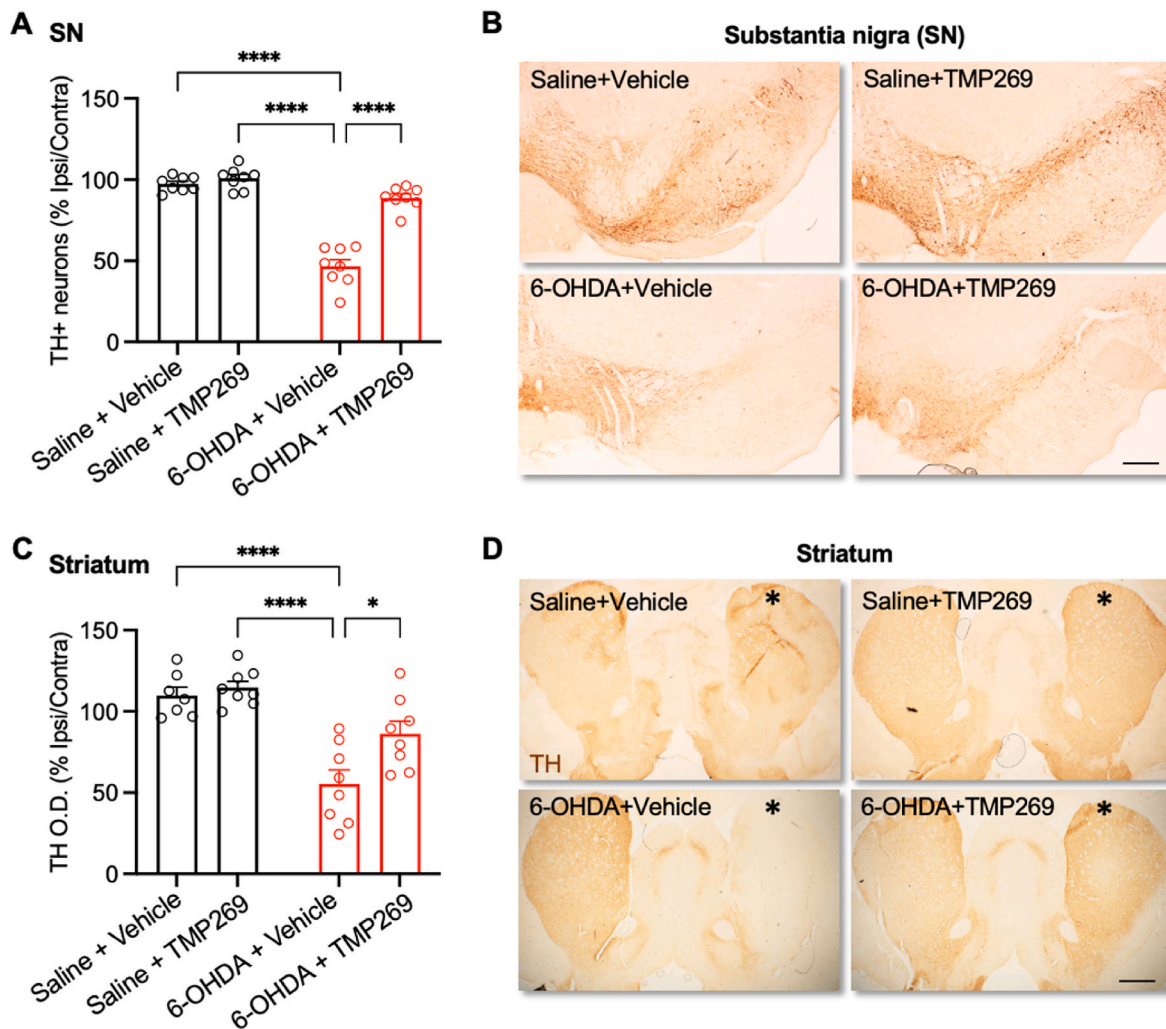
Fig. Peripheral administration of TMP269 protects against 6-OHDA-induced nigrostriatal degeneration in a rat model of PD. **(A)** Quantification of TH-immunopositive cells in the ipsilateral substantia nigra (SN) expressed as percentage of the contralateral side. **(B)** Representative photomicrographs of TH-immunostained sections through the ipsilateral SN. **(C)** Quantification of TH immunoreactivity in the ipsilateral striatum expressed as percentage of the contra-lateral side. **(D)** Representative photomicrographs of TH-immunostained sections through both striata; the lesioned side is indicated by an asterix (*). All data are presented as the mean ± SEM of n = 7–8 per group. ****$p < 0.0001$, *$p < 0.05$ vs. control or as indicated; Two-way ANOVA with post-hoc Bonferroni's test. Scale bar = **(B)** 500 μm and **(D)** 1000 μm.

4. Discussion

In this study we have shown that TMP269 protects against 6-OHDA-induced degeneration *in vitro* and *in vivo*. Furthermore, we have shown that TMP269 increases BMP2 and BMP-Smad signalling which is required for its beneficial effects. Firstly, we showed that treatment with 0.1 μM TMP269 increased histone H3 Lysine 9 (AcH3.K9.K14) acetylation and reduced HDAC5 enzymatic activity. In support of this, TMP269 has been reported to be highly selective for class IIa HDAC inhibition (Lobera et al., 2013). Furthermore, Lobera et al. observed that TMP269 was well tolerated *in vitro*, with no impact on mitochondrial activity and viability of human CD4$^+$ T cells when treated at concentrations as high as 10 μM (Lobera et al., 2013). Overall this suggests that TMP269 is a potent and highly selective class IIa HDAC inhibitor.

We analysed the effects of TMP269 on neurite growth in SH-SY5Y cells (Xicoy et al., 2017) as an *in vitro* analogue of *in vivo* pathological axonal degeneration (Hegarty et al., 2016). We found that 0.1 μM of TMP269 protected against 6-OHDA-induced neurite degeneration, and did not negatively affect cellular viability in concurrent and delayed treatment paradigms. This neuroprotective effect of TMP269 was further confirmed in differentiated SH-SY5Ys using a combination of

retinoic acid and BDNF to induce a dopaminergic phenotype (Taylor-Whiteley et al., 2019), and in primary dopaminergic neurons derived from the E14 rat ventral mesencephalon (VM) cultures. In agreement with this, previous studies have shown that class IIa HDACs, including HDAC5, have the ability to shuttle between the cytoplasm and the nucleus, affecting their function (Alchini et al., 2017; Cho and Cavalli, 2012; Ha et al., 2008; Pita-Thomas et al., 2019). HDAC5 nuclear or cytoplasmic localisation has been shown to be altered in response to cellular damage or pathogen administration, suggesting a role of HDAC5 the cellular response to injury (Pita-Thomas et al., 2019). We have previously reported that 6-OHDA induced increases in nuclear HDAC5, which reduces levels of AcH3.K9.K14 (Mazzocchi et al., 2021). Overall, this suggests that class-IIa HDACs may contribute to PD pathology and is consistent with the fact that TMP269 was neuroprotective.

In terms of mechanisms, HDAC5 has also been shown to regulate BMP2 expression by binding to the BMP2 promoter (Taniguchi et al., 2017), which is a dopaminergic neurotrophic factor (Goulding et al., 2019). In agreement with these data, we found that TMP269 upregulated BMP2 and that this increase was maintained in the presence of 6-OHDA. Furthermore, we also found increases in phosphorylated Smad1 (pSmad1), and BMP-Smad-dependent transcription, all of which
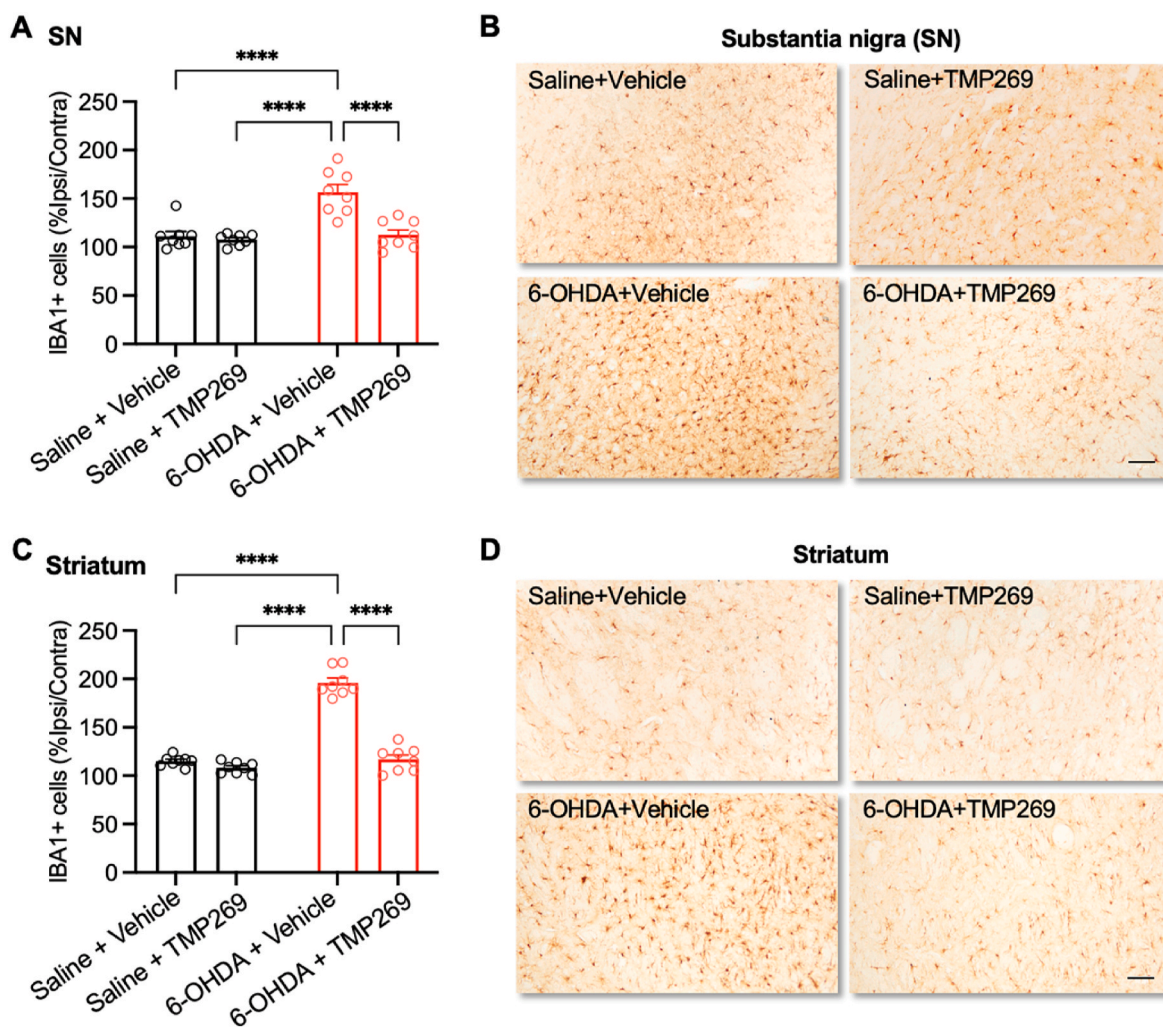
Fig. 8. Peripheral administration of TMP269 prevents microglial activation in 6-OHDA-lesioned rats. **(A)** Quantification of the number of IBA1-immunopositive cells per field in the ipsilateral substantia nigra (SN) expressed as percentage of the contralateral side in all treatment groups. **(B)** Representative photomicrographs of IBA1-immunopositive cells through the ipsilateral SN. **(C)** Quantification of the number of IBA1-immunopositive cells per field in the ipsilateral striatum expressed as percentage of the contralateral side in all treatment groups. **(D)** Representative photomicrographs of IBA1-immunopositive cells through the ipsilateral striatum. All data are presented as the mean ± SEM of n = 8 per group. ****p < 0.0001, vs. control or as indicated. Two-way ANOVA with *post-hoc* Tukey's test. Scale bar = 50 μm.

suggests increased BMP-Smad pathway activation in TMP269 treated cells (O'Keeffe et al., 2017). In agreement with the *in vitro* data, we also found corresponding 6-OHDA-induced reductions in BMP2 and pSmad1/5 levels in TH-positive DA neurons in the SN *in vivo,* that were restored by TMP269 treatment.

Interestingly, BMP2 has been recently reported to play a key role in the development of midbrain dopaminergic neurons, particularly in the nigrostriatal dopaminergic pathway (Hegarty et al., 2013; Terauchi et al., 2023). A BMP2-BMPR-Smad1 axis has been shown to promote dopaminergic synaptogenesis during development in a pathway specific establishment of nigrostriatal projections (Terauchi et al., 2023). Furthermore, Smad1cKO mice have shown reduced motor activity, suggesting a role for Smad1 in the maintenance of DA synapses. The specificity and importance of this BMP2-BMPR-Smad1 axis in both the development and maintenance of the nigrostriatal DA pathway, and in DA synaptic activity, suggests its activation could play an important role in the protection or regeneration of DA neurons in the pathological context of PD. Indeed, activation of the BMP-Smad signalling pathway has previously been shown to have protective effects in both *in vitro* and *in vivo* PD models. Previous studies have shown that BMP2 is protective against 6-OHDA-induced degeneration *in vitro* (Goulding et al., 2019) and *in vivo* (Espejo et al., 1999). In addition, other members of the BMP

family have been shown to protect against αSyn-induced neuronal degeneration *in vivo* (Goulding et al., 2021; Vitic et al., 2021). Overall, this suggests that activation of the BMP-Smad signalling pathway by TMP269 may underlie the beneficial effects of TMP269 against 6-OHDA-induced degeneration. This is supported by the *in vitro* experiments in which we used a selective inhibitor of the BMP-Smad pathway, dorsomorphin, which acts to inhibit the BMP-Smad pathway through the selective inhibition of the type 1 BMP receptors (Morizane et al., 2011). Dorsomorphin prevented the neuroprotective effects of TMP269 against 6-OHDA-induced degeneration in SH-SY5Y cells, suggesting that its effects are mediated through activation of the BMP-Smad signalling pathway.

Having established the protective effects of TMP269 *in vitro*, we also administered TMP269, or vehicle, peripherally over a period of 7 days via continuous subcutaneous infusion by mini osmotic pump to rats which had received either a sham or 6-OHDA striatal lesion. Peripheral administration was chosen due to the small molecule structure of TMP269. It has been established that small molecules which have molecular mass under 400 Da–500 Da undergo significant free diffusion across the blood-brain barrier (BBB) (Mikitsh and Chacko, 2014); the potential translational benefits of this, as peripheral administration is a much less invasive mode of delivery for a potential therapy. We
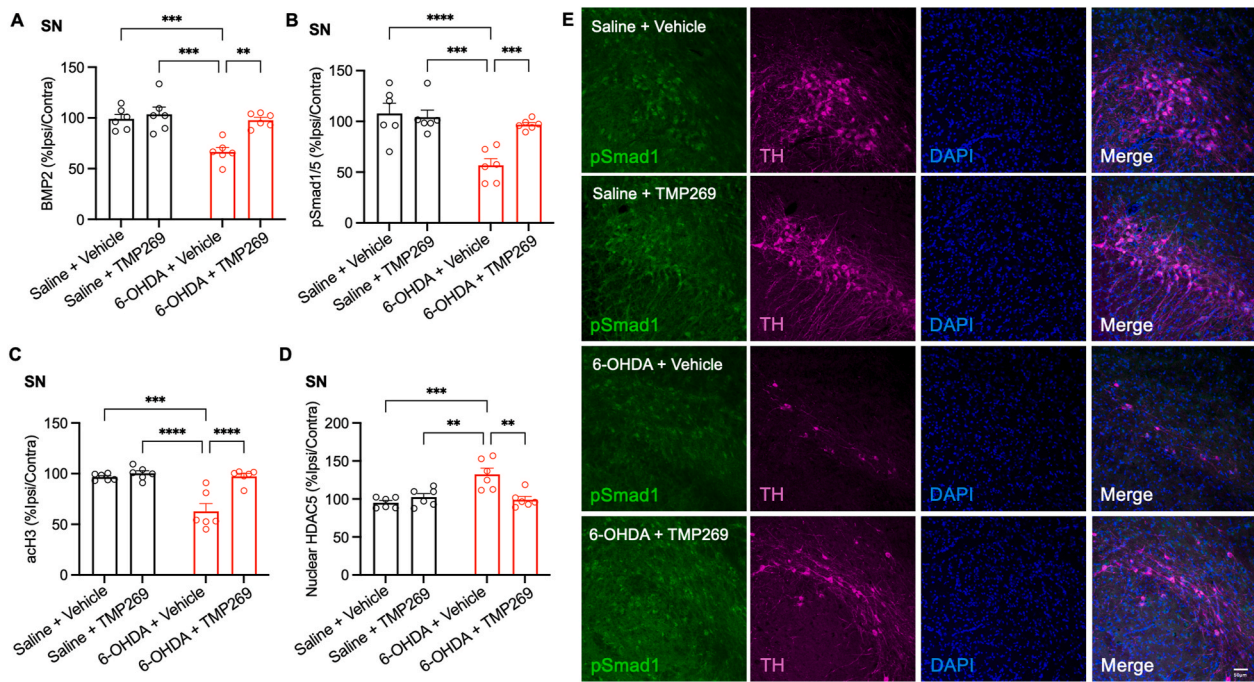
Fig. 9. Peripheral administration of TMP269 prevents 6-OHDA-induced changes in BMP2, pSmad1/5, acetylated histone 3 and HDAC5 in the SN *in vivo*. **(A–D)** Quantification of **(A)** BMP2, (B) pSmad1/5, **(C)** nuclear HDAC5 and **(D)** acetylated (ac)H3 expression in TH-positive neurons in the ipsilateral substantia nigra (SN) expressed as percentage of the contralateral side. (E) Representative images of phosho (p)Smad1/5 (green), TH (pink), DAPI (blue) in the SN. All data are presented as the mean ± SEM of n = 6 per group. **p < 0.01, ***p < 0.001, ****p < 0.0001 vs. control or as indicated. Two-way ANOVA with *post-hoc* Tukey's test. Scale bar = 50 μm.

observed improved motor function and significant protection of striatal dopaminergic innervation and of numbers of TH-positive neurons in the SN, indicating that TMP269 protected against 6-OHDA-induced nigrostriatal degeneration *in vivo*. The demonstration that 6-OHDA increased nuclear HDAC5 and reduced acetylated H3 levels in TH-positive neurons in the SN is indirect evidence of target engagement, and justifies a full pharmacokinetic study that is beyond the scope of the current investigation.

In the wider context, short chain fatty acids (SCFAs) are produced endogenously in the gut as bacterial-derived metabolites and act as pan-HDAC inhibitors (Mann et al., 2024). Furthermore, SCFA levels have been reported to be dysregulated in PD, leading to the investigation of SCFA dysregulation as a potential pathology-progressing mechanism, and of administration of SCFAs as potential disease-modifying therapies (Metzdorf and Tönges, 2021). Peripheral administration of the SCFA, sodium butyrate (NaB) ,has been shown to protect against MPTP-induced neuronal degeneration in C57BL/6J mice, to improve disruptions to the BBB, and to protect against apoptosis by upregulation of the anti-apoptotic factor BCL2 and downregulation of Bax (Hou et al., 2021; Liu et al., 2017). Another SCFA, sodium valproate, which was developed and is routinely used as an anticonvulsant medication for the treatment of epilepsy, has been reported to protect against dopaminergic degeneration induced by the irreversible proteasome inhibitor lactacystin, resulting in significant dose-dependent upregulation of the neurotrophic factors BDNF and GDNF, as well as BCL2 (Harrison et al., 2015). Other studies have also utilised more targeted HDAC inhibition of individual HDACs. One study used Tubastatin A to selectively inhibit the class IIb HDAC, HDAC6, resulting in significant protection against α-synuclein- induced neurodegeneration, by upregulation of chaperone-mediated autophagy and reduction of phosphorylation of α-synuclein at serine 129 (Francelle et al., 2020). Peripheral administration of the class IIa HDAC inhibitor MC1568 was also shown to protect against 6-OHDA induced degeneration and to limit 6-OHDA-induced increase in the numbers of IBA1-positive cells in the SN and striatum (Mazzocchi et al., 2022). In agreement with this, we also found that TMP269 prevented the 6-OHDA-induced increase in IBA1-positive microglia. Whether this effect of TMP269 is direct (has a direct action on microglia) or indirect (preventing neuronal injury, thereby preventing the microglial response) is an important line of future investigation. Taken together, these data indicate that pharmacological inhibition of HDACs, including class-IIa HDACs, have significant neuroprotective and potentially anti-neuroinflammatory potential, to protect against degeneration *in vivo* in PD models.

Overall, our collective findings in this study have significant translational implications in terms of the potential of TMP269 and its ability to protect against 6-OHDA-induced dopaminergic neuronal degeneration in models of PD. Additional work is required to further assess the neuroprotective potential of TMP269 in PD, namely assessing whether TMP269 treatment has beneficial effects in an α-synuclein *in vivo* model of PD. In conclusion, the data presented in the current study rationalise the continued investigation of pharmacological approaches to class-IIa HDAC inhibition towards the development of pharmacological neuroprotective therapies for PD that can be administered peripherally.

CRediT authorship contribution statement

Declaration of competing interest

All authors have no competing interests to declare.

Acknowldgement

Data availability

Data will be made available on request.

References

Alchini, R., Sato, H., Matsumoto, N., Shimogori, T., Sugo, N., Yamamoto, N., 2017. Nucleocytoplasmic shuttling of histone deacetylase 9 controls activity-dependent thalamocortical axon branching. Sci. Rep. 7, 6024. https://doi.org/10.1038/s41598-017-06243-7.

Anantha, J., Goulding, S.R., Tuboly, E., O'mahony, A.G., Moloney, G.M., Lomansey, G., Mccarthy, C.M., Collins, L.M., Sullivan, A.M., O'keeffe, G.W., 2022. NME1 protects against neurotoxin-, alpha-synuclein- and LRRK2-induced neurite degeneration in cell models of Parkinson's disease. Mol. Neurobiol. 59, 61–76.

Anwer, D.M., Gubinelli, F., Kurt, Y.A., Sarauskyte, L., Jacobs, F., Venuti, C., Sandoval, I. M., Yang, Y., Stancati, J., Mazzocchi, M., Brandi, E., O'Keeffe, G., Steece-Collier, K., Li, J., Deierborg, T., Manfredsson, F.P., Davidsson, M., Heuer, A., 2023. A comparison of machine learning approaches for the quantification of microglial cells in the brain of mice, rats and non-human primates. PLoS One 18 (5), e0284480. https://doi.org/10.1371/journal.pone.0284480.

Bloem, B.R., Okun, M.S., Klein, C., 2021. Parkinson's disease. Lancet 397, 2284–2303.

Cho, Y., Cavalli, V., 2012. HDAC5 is a novel injury-regulated tubulin deacetylase controlling axon regeneration. EMBO J. 31, 3063–3078. https://doi.org/10.1038/emboj.2012.160.

Choong, C.J., Sasaki, T., Hayakawa, H., Yasuda, T., Baba, K., Hirata, Y., Uesato, S., Mochizuki, H., 2016. A novel histone deacetylase 1 and 2 isoform-specific inhibitor alleviates experimental Parkinson's disease. Neurobiol. Aging 37, 103–116.

Collins, L.M., Adriaanse, L.J., Theratile, S.D., Hegarty, S.V., Sullivan, A.M., O'keeffe, G. W., 2015. Class-IIa histone deacetylase inhibition promotes the growth of neural processes and protects them against neurotoxic insult. Mol. Neurobiol. 51, 1432–1442.

Cordner, R.D., Friend, L.N., Mayo, J.L., Badgley, C., Wallmann, A., Stallings, C.N., Young, P.L., Miles, D.R., Edwards, J.G., Bridgewater, L.C., 2017. The BMP2 nuclear variant, nBMP2, is expressed in mouse hippocampus and impacts memory. Sci. Rep. 7, 46464.

Dai W, Qiao X, Fang Y, Guo R, Bai P, Liu S, Li T, Jiang Y, Wei S, Na Z, Xiao X, Li D. Signal Epigenetics-targeted drugs: current paradigms and future challenges. Transduct Target Ther. 9(1), 332. doi: 10.1038/s41392-024-02039-0.

Espejo, M., Cutillas, B., Ventura, F., Ambrosio, S., 1999. Exposure of foetal mesencephalic cells to bone morphogenetic protein-2 enhances the survival of dopaminergic neurones in rat striatal grafts. Neurosci. Lett. 275, 13–16.

Fahn, S., Oakes, D., Shoulson, I., Kieburtz, K., Rudolph, A., Lang, A., Olanow, C.W., Tanner, C., Marek, K., Parkinson Study, G., 2004. Levodopa and the progression of Parkinson's disease. N. Engl. J. Med. 351, 2498–2508.

Francelle, L., Outeiro, T.F., Rappold, G.A., 2020. Inhibition of HDAC6 activity protects dopaminergic neurons from alpha-synuclein toxicity. Sci. Rep. 10, 6064. https://doi.org/10.1038/s41598-020-62678-5.

Goulding, S.R., Concannon, R.M., Morales-Prieto, N., Villalobos-Manriquez, F., Clarke, G., Collins, L.M., Levesque, M., Wyatt, S.L., Sullivan, A.M., O'keeffe, G.W., 2021. Growth differentiation factor 5 exerts neuroprotection in an alpha-synuclein rat model of Parkinson's disease. Brain 144, e14. https://doi.org/10.1093/brain/awaa367.

Goulding, S.R., Sullivan, A.M., O'Keeffe, G.W., Collins, L.M., 2019. Gene co-expression analysis of the human substantia nigra identifies BMP2 as a neurotrophic factor that can promote neurite growth in cells overexpressing wild-type or A53T α-synuclein. Parkinsonism Relat. Disorders 64, 194–201. https://doi.org/10.1016/j.parkreldis.2019.04.008.

Grozinger, C.M., Hassig, C.A., Schreiber, S.L., 1999. Three proteins define a class of human histone deacetylases related to yeast Hda1p. Proc. Natl. Acad. Sci. U. S. A. 96 (9), 4868–4873. https://doi.org/10.1073/pnas.96.9.4868.

Guida, N., Laudati, G., Mascolo, L., Cuomo, O., Anzilotti, S., Sirabella, R., Santopaolo, M., Galgani, M., Montuori, P., Di Renzo, G., Canzoniero, L.M., Formisano, L., 2016. MC1568 inhibits thimerosal-induced apoptotic cell death by preventing HDAC4 up-regulation in neuronal cells and in rat prefrontal cortex. Toxicol. Sci. 154, 227–240.

Gupta, R., Ambasta, R.K., Kumar, P., 2020. Pharmacological intervention of histone deacetylase enzymes in the neurodegenerative disorders. Life Sci. 243, 117278.

Ha, C.H., Wang, W., Jhun, B.S., Wong, C., Hausser, A., Pfizenmaier, K., McKinsey, T.A., Olson, E.N., Jin, Z.-G., 2008. Protein kinase D-dependent phosphorylation and nuclear export of histone deacetylase 5 mediates vascular endothelial growth factor-induced gene expression and angiogenesis. J. Biol. Chem. 283, 14590–14599. https://doi.org/10.1074/jbc.M800264200.

Harrison, I.F., Crum, W.R., Vernon, A.C., Dexter, D.T., 2015. Neurorestoration induced by the HDAC inhibitor sodium valproate in the lactacystin model of Parkinson's is associated with histone acetylation and up-regulation of neurotrophic factors. Br. J. Pharmacol. 172, 4200–4215. https://doi.org/10.1111/bph.13208.

Harrison, I.F., Powell, N.M., Dexter, D.T., 2019. The histone deacetylase inhibitor nicotinamide exacerbates neurodegeneration in the lactacystin rat model of Parkinson's disease. J. Neurochem. 148, 136–156.

Hegarty, S.V., Collins, L.M., Gavin, A.M., Roche, S.L., Wyatt, S.L., Sullivan, A.M., O'keeffe, G.W., 2014. Canonical BMP-Smad signalling promotes neurite growth in rat midbrain dopaminergic neurons. NeuroMolecular Med. 16, 473–489.

Hegarty, S.V., Sullivan, A.M., O'Keeffe, G.W., 2013. BMP2 and GDF5 induce neuronal differentiation through a Smad dependant pathway in a model of human midbrain dopaminergic neurons. Mol. Cell. Neurosci. 56, 263–271. https://doi.org/10.1016/j.mcn.2013.06.006.

Hegarty, S.V., Sullivan, A.M., O'Keeffe, G.W., 2016. Protocol for evaluation of neurotrophic strategies in Parkinson's disease-related dopaminergic and sympathetic neurons in vitro. J. Biol. Methods 3, e50. https://doi.org/10.14440/jbm.2016.124.

Hegarty, S.V., Wyatt, S.L., Howard, L., Stappers, E., Huylebroeck, D., Sullivan, A.M., O'Keeffe, G.W., 2017. Zeb2 is a negative regulator of midbrain dopaminergic axon growth and target innervation. Sci. Rep. 7, 8568. https://doi.org/10.1038/s41598-017-08900-3.

Hou, Y., Li, X., Liu, C., Zhang, M., Zhang, X., Ge, S., Zhao, L., 2021. Neuroprotective effects of short-chain fatty acids in MPTP induced mice model of Parkinson's disease. Exp. Gerontol. 150, 111376. https://doi.org/10.1016/j.exger.2021.111376.

Jian, W., Wei, X., Chen, L., Wang, Z., Sun, Y., Zhu, S., Lou, H., Yan, S., Li, X., Zhou, J., Zhang, B., 2017. Inhibition of HDAC6 increases acetylation of peroxiredoxin1/2 and ameliorates 6-OHDA induced dopaminergic injury. Neurosci. Lett. 658, 114–120.

Johnston, T.H., Huot, P., Damude, S., Fox, S.H., Jones, S.W., Rusche, J.R., Brotchie, J.M., 2013. RGFP109, a histone deacetylase inhibitor attenuates L-DOPA-induced dyskinesia in the MPTP-lesioned marmoset: a proof-of-concept study. Parkinsonism Relat. Disorders 19, 260–264.

Kalia, L.V., Kalia, S.K., Lang, A.E., 2015. Disease-modifying strategies for Parkinson's disease. Mov. Disord. 30, 1442–1450.

Kirik, D., Rosenblad, C., Björklund, A., 1998. Characterization of behavioral and neurodegenerative changes following partial lesions of the nigrostriatal dopamine system induced by intrastriatal 6-hydroxydopamine in the rat. Exp. Neurol. 152, 259–277. https://doi.org/10.1006/exnr.1998.6848.

Li, B., Yang, Y., Wang, Y., Zhang, J., Ding, J., Liu, X., Jin, Y., Lian, B., Ling, Y., Sun, C., 2021. Acetylation of NDUFV1 induced by a newly synthesized HDAC6 inhibitor HGC rescues dopaminergic neuron loss in Parkinson models. iScience 24, 102302.

Li, J., Yu, C., Shen, F., Cui, B., Liu, N., Zhuang, S., 2022. Class IIa histone deacetylase inhibition ameliorates acute kidney injury by suppressing renal tubular cell apoptosis and enhancing autophagy and proliferation. Front. Pharmacol. 13, 946192.

Liu, J., Wang, F., Liu, S., Du, J., Hu, X., Xiong, J., Fang, R., Chen, W., Sun, J., 2017. Sodium butyrate exerts protective effect against Parkinson's disease in mice via stimulation of glucagon like peptide-1. J. Neurol. Sci. 381, 176–181. https://doi.org/10.1016/j.jns.2017.08.3235.

Lobera, M., Madauss, K.P., Pohlhaus, D.T., Wright, Q.G., Trocha, M., Schmidt, D.R., Baloglu, E., Trump, R.P., Head, M.S., Hofmann, G.A., Murray-Thompson, M., Schwartz, B., Chakravorty, S., Wu, Z., Mander, P.K., Kruidenier, L., Reid, R.A., Burkhart, W., Turunen, B.J., Rong, J.X., Wagner, C., Moyer, M.B., Wells, C., Hong, X., Moore, J.T., Williams, J.D., Soler, D., Ghosh, S., Nolan, M.A., 2013. Selective class IIa histone deacetylase inhibition via a nonchelating zinc-binding group. Nat. Chem. Biol. 9, 319–325. https://doi.org/10.1038/nchembio.1223.

Mai, A., Massa, S., Pezzi, R., Simeoni, S., Rotili, D., Nebbioso, A., Scognamiglio, A., Altucci, L., Loidl, P., Brosch, G., 2005. Class II (IIa)-selective histone deacetylase inhibitors. 1. Synthesis and biological evaluation of novel (aryloxopropenyl)pyrrolyl hydroxyamides. J. Med. Chem. 48, 3344–3353.

Mann, E.R., Lam, Y.K., Uhlig, H.H., 2024. Short-chain fatty acids: linking diet, the microbiome and immunity. Nat. Rev. Immunol. 24, 577–595. https://doi.org/10.1038/s41577-024-01014-8.

Mazzocchi, M., Collins, L.M., Sullivan, A.M., O'keeffe, G.W., 2020. The class II histone deacetylases as therapeutic targets for Parkinson's disease. Neuronal Signal. 4, NS20200001.

Mazzocchi, M., Goulding, S.R., Morales-Prieto, N., Foley, T., Collins, L.M., Sullivan, A.M., O'Keeffe, G.W., 2022. Peripheral administration of the Class-IIa HDAC inhibitor MC1568 partially protects against nigrostriatal neurodegeneration in the striatal 6-OHDA rat model of Parkinson's disease. Brain Behav. Immun. 102, 151–160. https://doi.org/10.1016/j.bbi.2022.02.025.

Mazzocchi, M., Goulding, S.R., Wyatt, S.L., Collins, L.M., Sullivan, A.M., O'Keeffe, G.W., 2021. LMK235, a small molecule inhibitor of HDAC4/5, protects dopaminergic neurons against neurotoxin- and α-synuclein-induced degeneration in cellular models of Parkinson's disease. Mol. Cell. Neurosci. 115, 103642. https://doi.org/10.1016/j.mcn.2021.103642.

Mazzocchi, M., Wyatt, S.L., Mercatelli, D., Morari, M., Morales-Prieto, N., Collins, L.M., Sullivan, A.M., O'keeffe, G.W., 2019. Gene Co-expression analysis identifies histone deacetylase 5 and 9 expression in midbrain dopamine neurons and as regulators of neurite growth via bone morphogenetic protein signaling. Front. Cell Dev. Biol. 7, 191.

Metzdorf, J., Tönges, L., 2021. Short-chain fatty acids in the context of Parkinson's disease. Neural Regen. Res. 16, 2015. https://doi.org/10.4103/1673-5374.308089.

Mikitsh, J.L., Chacko, A.-M., 2014. Pathways for small molecule delivery to the central nervous system across the blood-brain barrier. Perspect. Med. Chem. 6, 11–24. https://doi.org/10.4137/PMC.S13384.

Morizane, A., Doi, D., Kikuchi, T., Nishimura, K., Takahashi, J., 2011. Small-molecule inhibitors of bone morphogenic protein and activin/nodal signals promote highly efficient neural induction from human pluripotent stem cells. J. Neurosci. Res. 89, 117–126. https://doi.org/10.1002/jnr.22547.

O'Keeffe, G.W., Hegarty, S.V., Sullivan, A.M., 2017. Targeting bone morphogenetic protein signalling in midbrain dopaminergic neurons as a therapeutic approach in Parkinson's disease. Neuronal Signal. 1, NS20170027. https://doi.org/10.1042/NS20170027.

Olsson, M., Nikkhah, G., Bentlage, C., Bjorklund, A., 1995. Forelimb akinesia in the rat Parkinson model: differential effects of dopamine agonists and nigral transplants as assessed by a new stepping test. J. Neurosci. 15, 3863–3875.

Osorio, C., Chacon, P.J., Kisiswa, L., White, M., Wyatt, S., Rodriguez-Tebar, A., Davies, A.M., 2013. Growth differentiation factor 5 is a key physiological regulator of dendrite growth during development. Development 140, 4751–4762.

Park, G., Tan, J., Garcia, G., Kang, Y., Salvesen, G., Zhang, Z., 2016. Regulation of histone acetylation by autophagy in Parkinson disease. J. Biol. Chem. 291, 3531–3540.

Pinho, B.R., Reis, S.D., Guedes-Dias, P., Leitao-Rocha, A., Quintas, C., Valentao, P., Andrade, P.B., Santos, M.M., Oliveira, J.M., 2016. Pharmacological modulation of HDAC1 and HDAC6 in vivo in a zebrafish model: therapeutic implications for Parkinson's disease. Pharmacol. Res. 103, 328–339.

Pita-Thomas, W., Mahar, M., Joshi, A., Gan, D., Cavalli, V., 2019. HDAC5 promotes optic nerve regeneration by activating the mTOR pathway. Exp. Neurol. 317, 271–283. https://doi.org/10.1016/j.expneurol.2019.03.011.

Rane, P., Shields, J., Heffernan, M., Guo, Y., Akbarian, S., King, J.A., 2012. The histone deacetylase inhibitor, sodium butyrate, alleviates cognitive deficits in pre-motor stage PD. Neuropharmacology 62, 2409–2412.

Schallert, T., Fleming, S.M., Leasure, J.L., Tillerson, J.L., Bland, S.T., 2000. CNS plasticity and assessment of forelimb sensorimotor outcome in unilateral rat models of stroke, cortical ablation, parkinsonism and spinal cord injury. Neuropharmacology 39, 777–787.

Scholl, C., Weibetamuller, K., Holenya, P., Shaked-Rabi, M., Tucker, K.L., Wolfl, S., 2012. Distinct and overlapping gene regulatory networks in BMP- and HDAC-controlled cell fate determination in the embryonic forebrain. BMC Genom. 13, 298.

Sharma, S., Sarathlal, K.C., Taliyan, R., 2019. Epigenetics in neurodegenerative diseases: the role of histone deacetylases. CNS Neurol. Disord.: Drug Targets 18, 11–18.

Su, L., Liang, D., Kuang, S.Y., Dong, Q., Han, X., Wang, Z., 2020. Neuroprotective mechanism of TMP269, a selective class IIA histone deacetylase inhibitor, after cerebral ischemia/reperfusion injury. Neural Regen. Res. 15, 277–284.

Taniguchi, M., Carreira, M.B., Cooper, Y.A., Bobadilla, A.C., Heinsbroek, J.A., Koike, N., Larson, E.B., Balmuth, E.A., Hughes, B.W., Penrod, R.D., Kumar, J., Smith, L.N., Guzman, D., Takahashi, J.S., Kim, T.K., Kalivas, P.W., Self, D.W., Lin, Y., Cowan, C.W., 2017. HDAC5 and its target gene, Npas4, function in the nucleus accumbens to regulate cocaine-conditioned behaviors. Neuron 96, 130–144 e136.

Taylor-Whiteley, T.R., Le Maitre, C.L., Duce, J.A., Dalton, C.F., Smith, D.P., 2019. Recapitulating Parkinson's disease pathology in a three-dimensional human neural cell culture model. Dis. Models Mechan. 12, dmm038042.

Terauchi, A., Yee, P., Johnson-Venkatesh, E.M., Seiglie, M.P., Kim, L., Pitino, J.C., Kritzer, E., Zhang, Q., Zhou, J., Li, Y., Ginty, D.D., Lee, W.-C.A., Umemori, H., 2023. The projection-specific signals that establish functionally segregated dopaminergic synapses. Cell 186, 3845–3861.e24. https://doi.org/10.1016/j.cell.2023.07.023.

Thakur, P., Breger, L.S., Lundblad, M., Wan, O.W., Mattsson, B., Luk, K.C., Lee, V.M.Y., Trojanowski, J.Q., Bjorklund, A., 2017. Modelling Parkinson's disease pathology by combination of fibril seeds and alpha-synuclein overexpression in the rat brain. Proc. Natl. Acad. Sci. U. S. A. 114, E8284–E8293.

Vitic, Z., Safory, H., Jovanovic, V.M., Sarusi, Y., Stavsky, A., Kahn, J., Kuzmina, A., Toker, L., Gitler, D., Taube, R., Friedel, R.H., Engelender, S., Brodski, C., 2021. BMP5/7 protect dopaminergic neurons in an α-synuclein mouse model of Parkinson's disease. Brain 144, e15. https://doi.org/10.1093/brain/awaa368.

Wu, Q., Yang, X., Zhang, L., Zhang, Y., Feng, L., 2017. Nuclear accumulation of histone deacetylase 4 (HDAC4) exerts neurotoxicity in models of Parkinson's disease. Mol. Neurobiol. 54, 6970–6983. https://doi.org/10.1007/s12035-016-0199-2.

Xicoy, H., Wieringa, B., Martens, G.J.M., 2017. The SH-SY5Y cell line in Parkinson's disease research: a systematic review. Mol. Neurodegener. 12, 10. https://doi.org/10.1186/s13024-017-0149-0.

Ximenes, J.C., Neves, K.R., Leal, L.K., Do Carmo, M.R., Brito, G.A., Naffah-Mazzacoratti Mda, G., Cavalheiro, E.A., Viana, G.S., 2015. Valproic acid neuroprotection in the 6-OHDA model of Parkinson's disease is possibly related to its anti-inflammatory and HDAC inhibitory properties. J. Neurodegener Dis. 2015, 313702.

Yu, P.B., Hong, C.C., Sachidanandan, C., Babitt, J.L., Deng, D.Y., Hoyng, S.A., Lin, H.Y., Bloch, K.D., Peterson, R.T., 2008. Dorsomorphin inhibits BMP signals required for embryogenesis and iron metabolism. Nat. Chem. Biol. 4, 33–41.